

Mean Field and Capacity in Realistic Networks of Spiking Neurons Storing Sparsely Coded Random Memories

Emanuele Curti

curti@titanus.roma1.infn.it

INFM, Dipartimento di Fisica, Università di Roma La Sapienza, 00185 Rome, Italy

Gianluigi Mongillo

mongillo@surete3.roma1.infn.it

Dipartimento di Fisiologia Umana, Università di Roma La Sapienza, 00185 Rome, Italy

Giancarlo La Camera

lacamera@cns.unibe.ch

Institute of Physiology, University of Bern, 3012 Bern, Switzerland

Daniel J. Amit

daniel.amit@roma1.infn.it

INFM, Dipartimento di Fisica, Università di Roma La Sapienza, 00185 Rome, Italy, and Racah Institute of Physics, Hebrew University, Jerusalem, Israel

Mean-field (MF) theory is extended to realistic networks of spiking neurons storing in synaptic couplings of randomly chosen stimuli of a given low coding level. The underlying synaptic matrix is the result of a generic, slow, long-term synaptic plasticity of two-state synapses, upon repeated presentation of the fixed set of the stimuli to be stored. The neural populations subtending the MF description are classified by the number of stimuli to which their neurons are responsive (*multiplicity*). This involves $2p + 1$ populations for a network storing p memories. The computational complexity of the MF description is then significantly reduced by observing that at low coding levels (f), only a few populations remain relevant: the population of mean multiplicity $-pf$ and those of multiplicity of order \sqrt{pf} around the mean.

The theory is used to produce (predict) bifurcation diagrams (the onset of selective delay activity and the rates in its various stationary states) and to compute the storage capacity of the network (the maximal number of single items used in training for each of which the network can sustain a persistent, selective activity state). This is done in various regions of the space of constitutive parameters for the neurons and for the learning process. The capacity is computed in MF versus potentiation amplitude, ratio of potentiation to depression probability and coding level f . The MF results compare well with recordings of delay activity rate distributions in simulations of the underlying microscopic network of 10,000 neurons.

1 Introduction

Mean-field (MF) theory has provided a useful tool for obtaining fast and reliable insight into the stationary states (alias, persistent delay activity states, attractors, working memory) of recurrent neural networks. For networks of binary neurons—the Amari-Hopfield model (Amari, 1972; Hopfield, 1982), it allowed a very detailed description of the landscape of stationary states and even an accurate estimate of the storage capacity—the maximum number of memories that can be stored in the synaptic matrix and recalled (Amit, Gutfreund, & Sompolinsky, 1987; Amit, 1989). Its effectiveness is due to the high connectivity of the network (the large number of presynaptic contacts afferent on each neuron) and the relatively weak effect of a single neuron on another. Its precision is substantiated by detailed microscopic simulations.

The systematic MF study of the Amari-Hopfield model relied on two features: (1) the symmetry of the synaptic matrix, which allowed the application of techniques of statistical mechanics, and (2) the separability of synaptic efficacies, which allowed a description of the states of the network in terms of global, collective variables. These studies were extended to the storage of (0–1) neurons with low coding levels (Tsodyks & Feigelman, 1988; Buhmann, Divko, & Schulten, 1989) and to neurons with continuous response curves (Kuhn, 1990). In all these cases, it was found possible to describe the stationary states of the network in terms of collective variables, that is, in terms of population-averaged similarities (overlaps) of the state of the system and the memories embedded in the synapses.

The Willshaw model (Willshaw, Buneman, & Longuet-Higgins, 1969), which is fully symmetric, has not found an MF description due to the non-separability of its synaptic efficacies, except in the limit of low coding level and high storage (Golomb, Rubin, & Sompolinsky, 1990). As we show below, this treatment is a particular case of the approach we present: the limit of vanishing depression probability in training.

The experimental reality that such models capture is learned persistent selective delay spiking activity in temporal and prefrontal cortex (Miyashita & Chang, 1988; Miller, Erickson, & Desimone, 1996). To come nearer to the biological systems, the elements are chosen as spike-emitting units of two types, excitatory and inhibitory, occurring in different proportions and with different characteristics. The synaptic matrix connecting the neurons expresses the randomness of the connectivity, as well as the efficacies that existing synapses assume. In such networks, the afferent currents are driven by presynaptic spikes, and these currents feed the neural membrane depolarization. A neuron emits a spike whenever its depolarization crosses the threshold. Given a choice of the numbers of neurons of both types and their individual characteristics, as well as the synaptic matrix, the dynamics of the system can be simulated at the microscopic level. Such simulation serves as a substrate for recordings, upon presentation of stimuli in protocols representing various tasks, as would be the case for the corresponding experimental

situation (see, e.g., Amit, 1998). In such recordings one can register spike rasters for samples of neurons and monitor average rates (or higher-level statistics) on relevant time intervals, as is commonly done in experiments.

The space of parameters, though, is vast: for example, each type of neuron has several parameters, and the synapses of different types (excitatory-excitatory, excitatory-inhibitory, inhibitory-excitatory, inhibitory-inhibitory) can have different mean amplitudes and involve different delays. This renders a MF description quite essential. Scanning the parameter space to find realistic yet computationally interesting zones of parameters in microscopic simulations with a sensible number of spiking units (about 10,000) is computationally very intensive, while MF scanning of network state space is very rapid. This becomes even more pressing when one investigates the collective properties of learning, with dynamic plastic, spike-driven synapses.

The difficulty is that in more realistic situations, the synaptic matrix is strongly nonsymmetric, so there is no recourse to statistical mechanics. Nor can one expect a factorizable synaptic matrix. In the case considered here, the sparse and weak connectivity renders the neuronal firing rather weakly correlated. As a consequence, the high number of synaptic connections renders the afferent current to a neuron approximately gaussian and uncorrelated in time (for a step toward more general situations, see Brunel & Sergi, 1998; Fulvi Mari, 2000; Moreno & Parga, 2004). This allows for a MF description in terms of the average rates in functionally distinct populations (Amit & Brunel, 1997a).¹ In this situation, it is possible to pass from the dynamics of the depolarization of all neurons (in the microscopic description) to the dynamics (when slow) of the quantities driving the neural spike rates—the means and the variances per unit time of the afferent currents.² The dynamics of these quantities is driven by the rates of all neurons in the system. Given these two quantities for a given neuron, the average emission rate of the neuron is determined by its transduction function. Thus, the dynamics is closed, in that the rates determine the dynamics of the afferent currents, and those in turn determine the rates (Amit & Tsodyks, 1991; Amit, Brunel, & Tsodyks, 1994; Hopfield, 1984).

Thus far, the theory has been pursued only for the case of disjoint populations corresponding to different stimuli. In other words, each neuron was responsive to at most one visual stimulus.³

While this approach turned out to be useful and rather accurate in its results, compared with the microscopic simulations (Brunel, 2000), it suffered from several defects. First, the extremely sharp tuning curves are not

¹ For a precursor of this approach see, e.g., Wilson and Cowan (1972).

² In the following, we will refer to them as the mean and the variance, to retain the language used in Amit and Brunel (1997a).

³ *Visual* is used here in the restricted sense that cells in IT and PF express an elevated rate when visual stimuli are presented. These responses are not considered to be directly related to specific features of the visual objects.

realistic; neurons in experiments are rarely responsive to only one stimulus. Nor are they so selective in delay activity. Second, disjoint populations imply a very low storage capacity of the network. If the fraction of excitatory neurons in a selective population is f , one can store at most $1/f$ different stimuli in the network.

On the empirical side, progress in this field must cope with the finding of Miyashita and Chang (1988) and Miyashita (1988), who observed that a column 1 mm in diameter of IT cortex is able to sustain as many as 100 distinct, selective delay activity distributions, each employing about 2% to 3% of the cells in the column (Brunel, 1996). Each of these delay activity states corresponds to one fractal image. Hence, cells must be active in the delay activity state of more than one image, since $100 \times (2\text{--}3\%)$ is more than 100%.

Here we present an extension of the MF (population rate) dynamics to the case in which the populations selected (as responsive) for p different stimuli are selected at random. Hence, if the coding level is f , any two populations have a fraction f of each common to both (a fraction f^2 of the total number of cells); a fraction f^3 of the neurons in the network will be common, on average, to any three populations coding for different stimuli. The basic ideas have been suggested by La Camera (1999): to classify neurons in the network by the number of stimuli (of the training set) to which they are responsive (multiplicity of a cell) and by whether the selected stimulus is or is not among them. Previously, when one population was selected by a stimulus (either in response to stimuli or in selective delay activity), the excitatory neurons were divided into three homogeneous populations: one for the cells currently selected; one for all neurons selective to remaining stimuli and not currently selected, and one for all neurons not selective to any stimulus (background). Now there are $2p$ populations of excitatory neurons: p for selected neurons with all multiplicities $(1, \dots, p)$ and p for nonselected neurons, with all possible multiplicities $(0, \dots, (p-1))$. The latter include neurons of multiplicity 0 (not selective to any stimulus). Including inhibition, the MF dynamics would deal with $2p+1$ populations.

It is then verified that if average rates of cells within each of these $2p+1$ populations are equal and the synaptic matrix is generated in a rather organic learning process of long-term potentiation (LTP) and long-term depression (LTD) transitions between two discrete states of synaptic efficacy (Brunel, Carusi, & Fusi, 1998), the statistics of afferent currents (mean and variance) to the cells in each of these populations is equal, and hence these populations are natural candidates for MF analysis.

The approach is reinforced by observing that in the sparse coding limit, for any finite value of p , the number of populations that actually affect the afferents of all neurons is very much lower than $2p+1$. This is due to the fact that the number of neurons in a population varies strongly with the multiplicity of the population. In fact, when $f \ll 1$, this number is sharply peaked in populations with multiplicities around the mean pf . As a consequence, only a reduced number of relevant populations (of order \sqrt{pf})

contributes significantly to the feedback. The rates of neurons in all other populations are determined by the afferents from the relevant populations.

We first present a general description of the MF approach. Section 3 describes the methods used to derive and solve the full and reduced MF equations for the stationary states, as well as of the simulation process employed to test the MF predictions. These are followed by the results section, including MF bifurcation diagrams compared with simulation rates and the dependence of the critical capacity of the network on potentiation-to-depression efficacy, potentiation-to-depression probability, the inhibitory efficacy, and the coding level. In section 5, we consider prospects of the applications of the new approach as well as its relation with the Willshaw model.

2 Mean-Field Approach and Synaptic Structuring

2.1 Generalities. In this section, we recapitulate general ideas that allow for a network of spiking neurons to be described by collective variables, that is, mean rates in statistically homogeneous neural populations, and extend these ideas to the case of randomly chosen selectivity for stimuli and to a synaptic matrix generated by slow learning of many repeated presentations of such sets of stimuli. Section 3 will deal with the technical aspects of the resulting framework with a specific model for the spiking neuron.

The MF approach consists in dividing the network into distinct and statistically homogeneous subpopulations: a neuron belongs to at most one subpopulation, and two neurons belonging to the same subpopulation have the same statistics of afferent synapses. One then assumes that all neurons in the same subpopulation have an equal average spike emission rate. This renders the statistics of afferent currents homogeneous within each subpopulation. The statistics of the afferent currents in turn determines the average emission rate in the subpopulation. The steady mean emission rate in each subpopulation is obtained requiring self-consistency—that the output rates (generated by the transduction function) be equal to the input rates (which determine the input currents).

When neurons within the network respond to more than one stimulus, the subpopulations formed by collecting neurons responding to a given stimulus are in general not distinct. Cells responding to more than one stimulus belong to more than one subpopulation. The consequence is that these overlapping populations cannot be used to carry out a MF analysis, in the sense described above, as was done in Amit and Brunel (1997a). In order to obtain subpopulations suitable for MF analysis, we follow La Camera (1999) and lump together neurons responding to the same number of stimuli, regardless of their identity. These, we show next, solve the problem.

2.2 The Model. The model network is much as in Amit and Brunel (1997a). It is composed of N_E excitatory and N_I inhibitory spiking neurons. Each neuron receives, on average, C_E excitatory and C_I inhibitory synaptic

contacts from presynaptic neighbors (i.e., neurons with a direct afferent on the given neuron), randomly and independently selected. Neurons also receive C_{ext} excitatory contacts, with efficacy J_{ext} , coming from outside the network and carrying noise as well as signals of presented stimuli. They emit spikes independently, in a Poissonian process with mean rate v_{ext} .

Plasticity is restricted to the excitatory-to-excitatory (EE) synapses. An existing EE synapse has two possible efficacies: potentiated, J_p , or depressed, $J_d < J_p$. In this study, the distribution of the EE synapses is conceived as the outcome of a long, slow training stage, in which the p stimuli to be memorized are repeatedly presented in a random sequence. The synaptic distribution is kept fixed throughout the analysis (see below). The remaining synapses have fixed, unstructured efficacies. The distribution of these efficacies (mean and variance) depends on the type of pre- and postsynaptic neurons (EI, IE, II).

A stimulus is characterized by the set of excitatory neurons that are responsive to it. Of particular interest is the subset of cells whose rate is enhanced by the stimulus presentation to a level that can lead to synaptic plasticity. When the cell populations are selected at random, with a given coding level f (average fraction of cells in the assembly responsive to the stimulus), cells responsive to one stimulus may respond to another (fraction f^2) and to more than 2. Every cell can be characterized (uniquely) by specifying the list of stimuli it responds to and does not respond to. If the network has been exposed systematically to p stimuli, a cell is fully defined by the p -bit word, its response pattern, with 1 (0) at position k indicating that it is responsive (nonresponsive) to stimulus k . Thus, the p -bit word (0, 1, 1, 0, 0, \dots , 0) corresponding to a given cell indicates that the cell responds exclusively to stimuli 2, 3, and 4 out of p , although the rates are not necessarily equal. The number of 1's in the response pattern of a neuron will be called its multiplicity, α , β , \dots . It should be emphasized that the (0/1) are not the responses of the neurons to a stimulus, but merely shorthand for whether a neuron has a strong or weak response to the stimulus.

Consider two given cells and the synapse connecting them. The corresponding two p -bit response patterns determine what will occur to the synapse connecting them when a given stimulus is presented. The structuring process is envisaged to be stochastic and slow. If the bit corresponding to the stimulus is 1 in both response patterns and if the synapse is in its low state, the synapse will potentiate with probability q_+ , ($J_d \rightarrow J_p$, LTP); if the presynaptic bit is 1 and the postsynaptic is 0 and if the synapse is in its high state, the synapse will depress with probability q_- ($J_p \rightarrow J_d$, LTD);⁴ and if the presynaptic bit is 0, it will not change. In the following we use

$$q_+ = q, \quad q_- = f\rho q. \quad (2.1)$$

⁴ This LTD mechanism can be easily generalized. See, e.g., Brunel et al. (1998).

This scaling of q_-/q_+ optimizes network capacity (Amit & Fusi, 1994). ρ is a parameter of order 1, defined by equation 2.1, regulating the LTD-to-LTP probability ratio.

Suppose that during training, the p stimuli are shown at a uniform rate, with equal probability. The total number, P , of potentiation conditions (1,1) seen by a given synapse, and the total number D of depression conditions (0,1) is determined by the two p -bit response patterns corresponding to the two cells connected by it.

2.3 Asymptotic Synaptic Structuring. The synaptic dynamics is a Markov process. A random walk is induced among the two states of every synapse by the presentation of the stimuli. In general, the final state of the synapse, following a given sequence of stimuli, could depend on the order of presentation due to the fact that the synapse has only two states. If the transition probabilities are low (slow learning limit, small q_+ , q_-), the variability from sequence to sequence becomes negligible. What matters is the number of potentiating or depressing patterns seen by the synapse as a consequence of the presentation of the whole training set and not the order in which they occurred (Brunel et al., 1998). In this limit, the probability of finding a synapse in its potentiated state, J_p , is obtained by averaging over all possible realizations of the random sequences of presentation (Brunel et al., 1998), as

$$\gamma(P, D) = \frac{q_+ P}{q_+ P + q_- D} = \frac{P}{P + f\rho D}. \quad (2.2)$$

$P(D)$ is the number of potentiating (depressing) pairs of activity seen by the synapse as a consequence of the presentation of the sequence. This is the case (see equation 2.2) when at least one of the p stimuli tends to potentiate or depress the synapse. Otherwise, the synapse is not affected, and the final probability (i.e., following training) that the synapse be in the potentiated state coincides with the initial probability γ_0 (i.e., prior to training and uncorrelated with any of the stimuli), or

$$\gamma(P = 0, D = 0) = \gamma_0. \quad (2.3)$$

In the absence of depression (the limit $\rho \rightarrow 0$), the statistical description of the synaptic structuring (see equations 2.2 and 2.3) provides a description also for a Willshaw-like synaptic matrix. The formal correspondence is exact if $J_p = 1$, $J_d = 0$, and $\gamma_0 = 0$ (Willshaw et al., 1969). In this limit, equation 2.2 becomes

$$\lim_{\rho \rightarrow 0} \gamma(P, D) = \begin{cases} \gamma_0 & \text{if } P = 0 \\ 1 & \text{if } P > 0 \end{cases}. \quad (2.4)$$

Every synapse that experiences at least one potentiating pattern of activity is in its potentiated state with probability 1. Otherwise, it remains unstruc-

tured, that is, potentiated with probability γ_0 . In other words, the stimuli can potentiate only the synaptic efficacy. Thus, MF equations for a recurrent network with a Willshaw-like synaptic matrix (see, e.g., Golomb et al., 1990) can be obtained from the MF theory developed below, in the limit of vanishing ρ .

2.4 Afferent Currents and Multiplicity. Next, we show that cells with the same multiplicity form natural populations for a MF analysis. Note first that the average (replacing spikes by rates, e.g. Amit & Tsodyks, 1991) current afferent to neuron i from other excitatory neurons is

$$\langle I_i \rangle = \sum_j \langle J_{ij} \rangle v_j. \quad (2.5)$$

j goes over all presynaptic neurons. If neurons with the same multiplicity have the same mean emission rate, v_β , the sum can be rewritten as a sum over multiplicities,

$$\langle I_i \rangle = C_E \sum_\beta \langle J_{ij} \rangle_\beta \pi(\beta) v_\beta, \quad (2.6)$$

where C_E is the average EE connectivity, $\pi(\beta)$ is the probability that the presynaptic neuron is of multiplicity β , and $\langle J_{ij} \rangle_\beta$ is the average synaptic efficacy from a neuron of multiplicity β to postsynaptic neuron i . This last average of J_{ij} is over all possible presynaptic response patterns of neurons of multiplicity β .

It is given by

$$\langle J_{ij} \rangle_\beta = \sum_{P,D} [\gamma(P,D) J_p + (1 - \gamma(P,D)) J_d] \psi_\beta^i(P,D), \quad (2.7)$$

where $\gamma(P,D)$ is given by equations 2.2 and 2.3, and $\psi_\beta^{(i)}(P,D)$ is the joint probability distribution of P and D (in an average MF sense; (Brunel et al., 1998)).

Given the response pattern of neuron i (of multiplicity α), $\psi_\beta^i(P,D)$ can be determined (see below). Suppose, without loss of generality, that the postsynaptic neuron responds to the first α stimuli and that $\alpha < \beta$. The maximal value of P is α , since α is the maximal number of coincident active bits in the two response patterns. If $\alpha + \beta \leq p$, the minimal value of P is zero. If $\alpha + \beta > p$, there must be at least $\alpha + \beta - p$ coincident bits in the two response patterns. Hence, P ranges from 0 (or from $\alpha + \beta - p$ when $\alpha + \beta > p$) to α . The reasoning is analogous when $\alpha > \beta$, exchanging α and β .

The actual value of P is determined by the number of ones among the first α bits in the response pattern of the presynaptic cell. Each active bit in this

position will find a corresponding active bit in the response pattern of the postsynaptic cell. The corresponding value of D is the number of 1's among the remaining $p - \alpha$ bits of the response pattern of the presynaptic neuron: Each active bit in this position in the presynaptic response pattern will find an inactive bit in the response pattern of the postsynaptic cell. Because the presynaptic cell responds to just β stimuli, D is given by $D = \beta - P$.

There are $\binom{p}{\beta}$ possible response patterns for a neuron of multiplicity β .

Among these, $\binom{\alpha}{h} \binom{p-\alpha}{\beta-h}$ have h 1's among the first α bits and $\beta - h$ 1's among the remaining $p - \alpha$. For all these, $P = h$ and $D = \beta - h$. Hence, if neuron i is of multiplicity α ,

$$\psi_{\beta}^{(i)}(P, D) = \binom{\alpha}{P} \binom{p-\alpha}{D} / \binom{p}{\beta}, \quad \text{with } D = \beta - P, \quad (2.8)$$

depending only on the multiplicity α of the postsynaptic neuron and not on its particular response pattern. Replacing $\psi_{\beta}^{(i)}(P, D) \equiv \psi_{\alpha\beta}(P, D)$ in equation 2.7 and equation 2.7 in 2.6, for the afferent current, we find

$$\mu_{\alpha} = C_E \sum_{\beta} J_{\alpha\beta} \pi(\beta) v_{\beta}, \quad (2.9)$$

where μ_{α} is the mean current to a neuron of multiplicity α , while $J_{\alpha\beta}$ is given by

$$J_{\alpha\beta} = \sum_{P,D} [\gamma(P, D) J_p + (1 - \gamma(P, D)) J_d] \psi_{\alpha\beta}(P, D). \quad (2.10)$$

Thus, all neurons with the same multiplicity receive the same mean afferent current, with the same variance, provided the rates in a population of equal multiplicity are equal. Consequently, the cells in each such population would emit at the same mean emission rate, which expresses the consistency of the underlying assumption. In fact, the mean emission rate varies from neuron to neuron, mostly due to the random connectivity in the network. However, for large networks, the distribution of rates within a statistically homogeneous population is strongly peaked around its (population) mean value. This is confirmed by simulations (see below) and makes the cells with the same multiplicity a neural population suitable for MF analysis.

To exemplify the import of the above arguments we present in Figure 1 the average fraction of potentiated synapses afferent on a neuron, as a function of the multiplicity α of that neuron, defined as

$$\langle \gamma \rangle_{\alpha} = \sum_{\beta} \left(\sum_{P,D} \gamma(P, D) \psi_{\alpha\beta}(P, D) \right) \pi(\beta), \quad (2.11)$$

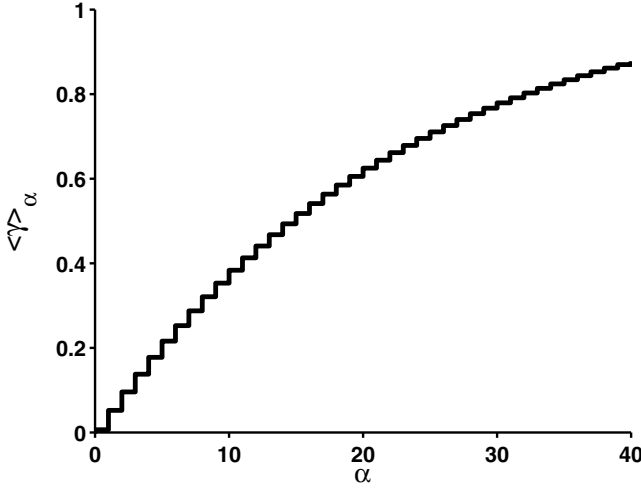


Figure 1: Sensitivity of afferent synaptic potentiation to neural multiplicity. Mean fraction of potentiated synapses versus postsynaptic multiplicity, in a network with $f = 0.05$, $\rho = 1$, and $p = 40$. This precludes the use of a single excitatory population for MF purposes.

with $\gamma(P, D)$ and $\psi_{\alpha\beta}(P, D)$ given by equations 2.2 and 2.8, respectively. As can be seen, the fraction of potentiated synapses varies with the multiplicity. Consequently, in a steady state, the mean emission rates of the neurons responding to the same stimulus are not homogeneous. They depend on the multiplicity of that neuron. Thus, the number of subpopulations of excitatory neurons of potentially different rates, required for MF analysis, is $p + 1$ —one for each multiplicity $(0, \dots, p)$.

The above discussion was limited to the case without selective activity. When neurons selective to a given stimulus are active, not all populations of a given multiplicity are expected to have the same rate. Those responsive to the stimulus will emit at a higher rate than the others within the same subpopulation. The arguments presented above can be extended (see the appendix), leading to the conclusion that $2p$ excitatory populations would be required, with rates v_β^s for selective neurons of multiplicity β and v_β^n for nonselective neurons of the same multiplicity. The resulting $2p$ populations consist of p nonselective ones, of multiplicity $0, 1, \dots, p - 1$, and p selective ones, of multiplicity $1, 2, \dots, p$. By contrast, in the case of nonoverlapping memories, the description of the retrieval state needs only three excitatory populations (selective with multiplicity 1 and nonselective neurons with multiplicities 0 or 1), regardless of the number of stored memories (Amit & Brunel, 1997a).

2.5 Mean-Field Analysis. To study whether the network can sustain single-item working memory states, we consider $2p+1$ populations, adding the population of inhibitory neurons to the $2p$ populations mentioned above. The mean currents to selective (s) and nonselective (n) neurons in the excitatory populations of multiplicity α ,

$$\begin{aligned}\mu_\alpha^s &= C_E \left[\sum_{\beta=1}^p J_{\alpha\beta}^{ss} \pi_s(\beta) v_\beta^s + \sum_{\beta=0}^{p-1} J_{\alpha\beta}^{sn} \pi_n(\beta) v_\beta^n \right] + \mu_I + \mu_{ext} \\ \mu_\alpha^n &= C_E \left[\sum_{\beta=1}^p J_{\alpha\beta}^{ns} \pi_s(\beta) v_\beta^s + \sum_{\beta=0}^{p-1} J_{\alpha\beta}^{nn} \pi_n(\beta) v_\beta^n \right] + \mu_I + \mu_{ext}.\end{aligned}\quad (2.12)$$

C_E is the average number of recurrent excitatory collaterals received by a neuron, $J_{\alpha\beta}^{ss}$ is the mean efficacy of synapses received by a selective neuron with multiplicity α from selective neurons with multiplicity β , and $J_{\alpha\beta}^{sn}$ is the mean efficacy received by a selective neuron with multiplicity α from nonselective neurons with multiplicity β . $J_{\alpha\beta}^{ns}$ and $J_{\alpha\beta}^{nn}$ are defined analogously; $\pi_s(\beta)$ ($\pi_n(\beta)$) is the probability that a selective (nonselective) neuron has multiplicity β ; v_β^s (v_β^n) is the mean emission rate in subpopulation of selective (nonselective) neurons of multiplicity β ; μ_I and μ_{ext} are, respectively, the mean afferent inhibitory current and the mean external current, given in equations A.13. The latter include the selective stimulus current.

Analogously, the variances of the afferent currents are obtained as

$$\begin{aligned}(\sigma_\alpha^s)^2 &= C_E \left[\sum_{\beta=1}^p \Delta J_{\alpha\beta}^{ss} \pi_s(\beta) v_\beta^s + \sum_{\beta=0}^{p-1} \Delta J_{\alpha\beta}^{sn} \pi_n(\beta) v_\beta^n \right] + \sigma_I^2 + \sigma_{ext}^2 \\ (\sigma_\alpha^n)^2 &= C_E \left[\sum_{\beta=1}^p \Delta J_{\alpha\beta}^{ns} \pi_s(\beta) v_\beta^s + \sum_{\beta=0}^{p-1} \Delta J_{\alpha\beta}^{nn} \pi_n(\beta) v_\beta^n \right] + \sigma_I^2 + \sigma_{ext}^2,\end{aligned}\quad (2.13)$$

where σ_I^2 and σ_{ext}^2 are, respectively, the variance of the inhibitory current and the variance of the external current, given in equations A.14. The $J_{\alpha\beta}^{xy}$, $\Delta J_{\alpha\beta}^{xy}$ and $\pi_x(\beta)$ are computed in the appendix.

Note that in computing the variance of the currents, we have ignored the correlations between synaptic efficacies that have a common presynaptic neuron. This is justified as long as the ratio between the correlated contribution to the variance is small compared to the uncorrelated one. This ratio is, for low f and high loading ($\sim 1/f^2$), $\sim C f^2 \cdot p f^2 \exp -2p f^2 \ll 1$ (see Amit & Fusi, 1994; Golomb et al., 1990). In our simulations, it is always $\ll 0.72$. Moreover, with our parameters, the variance of the afferent currents is dominated by the external and the inhibitory contributions, while the potential correlations affect exclusively the recurrent excitatory contribution.

The statistics of the current—its mean and variance—determines in turn the mean emission rate of the neuron according to

$$v_{\alpha}^{(s,n)} = \Phi(\mu_{\alpha}^{(s,n)}, \sigma_{\alpha}^{(s,n)}), \quad (2.14)$$

where the functional form of the transduction function $\Phi(\cdot)$ depends on the neural model chosen. The mean emission rates within the subpopulations determine the statistics of the afferent currents. Self-consistency then implies that the mean emission rates determining a given statistics of the currents be equal to the rates at which spikes are produced in the various subpopulations given those currents:

$$\begin{cases} v_{\alpha}^s = \Phi(\mu_{\alpha}^s(\{v_{\beta}^s, v_{\beta}^n\}), \sigma_{\alpha}^s(\{v_{\beta}^s, v_{\beta}^n\})) \\ v_{\alpha}^n = \Phi(\mu_{\alpha}^n(\{v_{\beta}^s, v_{\beta}^n\}), \sigma_{\alpha}^n(\{v_{\beta}^s, v_{\beta}^n\})) \end{cases} \quad (2.15)$$

$\mu_{\alpha}^x(\{v_{\beta}^s, v_{\beta}^n\})$, $\sigma_{\alpha}^x(\{v_{\beta}^s, v_{\beta}^n\})$ represent the dependence of the means and the variances of the afferent currents on all the population rates. The dependence on the inhibitory and the external emission rates is not explicitly indicated.

A solution of equations 2.15 provides the mean emission rates of all subpopulations in a stationary state of activity. The phenomenology one expects is (Amit & Brunel, 1997a):

- Spontaneous activity (SA). For low values of $J_p/J_d \sim 1$ there exists a single solution of equations 2.15 with $v_{\beta}^s = v_{\beta}^n$ for $\beta = 1, \dots, p-1$. In other words, selective and nonselective populations have the same mean emission rate. Rates may depend on the multiplicity of the cells, due to potentiations that did take place between certain groups of neurons. The system is ergodic. See section 4.
- Retrieval state or working memory (WM). Above some value of J_p/J_d , a bifurcation takes place, and besides the SA solution, a new solution of equations 2.15 appears with $v_{\beta}^s > v_{\beta}^n$ for $\beta = 1, \dots, p-1$. In this state, one population of neurons, responsive to a given stimulus, has elevated activity, and the remaining neurons, not selective to that stimulus, emit at low rates. But within each of the two populations (selective and not selective), the rates will depend on the multiplicity of the cells. There exist p different retrieval states, each for one of the learned stimuli.
- Destabilized SA. When J_p/J_d becomes too high, the spontaneous activity state becomes unstable and only selective delay activity states exist.

2.5.1 Reduced Mean Field. Since one expects the number of stored memories to become large, a system of $2p+1$ dynamical variables in mean field is still excessive and may become as large as the number of cells in the network, or larger. A further step, beyond the $2p+1$ reduction, can be achieved

by observing that $\pi_x(\beta)$ becomes negligible for values of β distant from the peak of the distribution, at fp . Disregarding selectivity for the sake of simplicity, $\pi(\beta)$ is

$$\pi(\beta) = \binom{p}{\beta} f^\beta (1-f)^{p-\beta}, \quad (2.16)$$

where $f^\beta (1-f)^{p-\beta}$ is the probability that a neuron respond to exactly β out of p stimuli. For large values of p , this distribution becomes gaussian, with mean and variance given by

$$\mu_p = fp, \quad \sigma_p^2 = f(1-f)p.$$

But if f is low enough, even for $pf \sim 2, 3$ the distribution is quite peaked, as we show below.

If, for example, one considers populations within 3σ of the peak, about 99% of the totality of excitatory neurons of the network are included. But $\sigma \sim \sqrt{fp}$, and hence this number of populations is quite low compared to $2p$. One then takes this reduced number of populations as the only ones that contribute to the currents, reducing the number of equations to be treated for self-consistency. The rates of neurons in the other populations are computed directly from the afferent currents produced by the populations retained. For example, for $f = 0.05$ and $p = 100$, $\sigma_p \simeq 2.24$, $3\sigma \sim 7$, and when selective and nonselective populations are considered, one needs only 24 populations instead of the initial 200.

3 Methods

3.1 Spiking Neuron Model. The underlying single unit in our network is the standard integrate-and-fire element, without adaptation. Membrane depolarization integrates the afferent current $I(t)$ according to

$$\dot{V} = -\frac{V}{\tau} + I(t), \quad (3.1)$$

where τ is the membrane time constant. Whenever the depolarization reaches a threshold θ , the cell emits a spike and remains refractory for a time τ_{arp} . Then V is reset to V_r and normal dynamics resumes. The current $I(t)$ to a neuron, produced by the afferent spikes, is

$$I(t) = I_{ext}(t) + \sum_j J_j \sum_k \delta(t - t_j^{(k)} - \delta_j), \quad (3.2)$$

where I_{ext} is the current coming from outside the network (see, e.g., Amit & Brunel, 1997a); j goes over the presynaptic sites; J_j is the efficacy of the corresponding synapse; k runs over all spikes arriving at a given site; $t_j^{(k)}$

is the emission time of the k th spike by neuron j ; and δ_j is the associated transmission delay. The effect of a spike is very brief.

When $I(t)$ is stationary, gaussian, and independent at different times, the transduction function of a neuron $\Phi(\cdot)$ is (Amit & Tsodyks, 1991; Ricciardi, 1977)

$$v = \Phi(\mu, \sigma) = \left(\tau_{app} + \tau \int_{\frac{v_r - \mu}{\sigma}}^{\frac{\theta - \mu}{\sigma}} \sqrt{\pi} e^{u^2} (1 + \operatorname{erf}(u)) du \right)^{-1}, \quad (3.3)$$

where μ and σ^2 are, respectively, the mean and the variance of the afferent current. Since in a randomly and weakly connected network, the afferent current is gaussian to a good approximation (Amit & Brunel, 1997b), we use equation 3.3 as the transduction function in our MF studies.

3.2 Stationary States in Mean Field

3.2.1 The Full Case. For most of the results obtained in MF, we used a simplified set of dynamical equations for the evolution of the rates. In the full case, we integrate the following $2p + 1$ equations (all multiplicities),

$$\begin{cases} \tau_E \dot{v}_\alpha^s(t) = -v_\alpha^s(t) + \Phi_E(\{v_\beta^s(t)\}, \{v_\beta^n(t)\}, v_I(t)), & \alpha = 1, \dots, p \\ \tau_E \dot{v}_\alpha^n(t) = -v_\alpha^n(t) + \Phi_E(\{v_\beta^s(t)\}, \{v_\beta^n(t)\}, v_I(t)), & \alpha = 0, \dots, p-1 \\ \tau_I \dot{v}_I(t) = -v_I(t) + \Phi_I(\{v_\beta^s(t)\}, \{v_\beta^n(t)\}, v_I(t)), \end{cases} \quad (3.4)$$

performing a first-order numerical integration, with a time step $\Delta t = 0.01$ ms (about 10^{-3} of the time constants involved). τ_E , τ_I are fictitious excitatory and inhibitory time constants, whose actual values are immaterial, since we consider only stationary states. We take them equal to the membrane time constants of the excitatory and inhibitory spiking neurons, respectively (see Table 1). $\{v_\beta^s(t)\}$, $\{v_\beta^n(t)\}$ are, respectively, the set of rates in the selective and nonselective populations of multiplicity β . The Φ 's are the transduction functions defined in equation 3.3. Their dependence on the type of neuron (excitatory and inhibitory) is via τ , V_r , and Θ . Their dependence on the rates is via the mean and variance of the afferent current to each type of neuron, equations 2.12 and 2.13.

We looked for the steady states of this dynamical system, which are the solutions of equations 2.15. The test for stationarity is that all $2p + 1$ rates, upon the next integration step, undergo a relative variation less than a given tolerance $\Delta_f \sim 10^{-6}$, that is,

$$\left| \frac{v_\alpha^x(t + \Delta t) - v_\alpha^x(t)}{v_\alpha^x(t)} \right| < \Delta_f.$$

The iterative approach to the stationary states, via equations like equation 3.4, guarantees their stability with respect to this dynamics.

Table 1: Parameters Used in MF Calculations and Simulations.

Single-Cell Parameters	E	I
θ —Spike emission threshold	20 mV	20 mV
V_r —Reset potential	10 mV	10 mV
τ —Membrane time constant	20 ms	10 ms
τ_{arp} —Absolute refractory period	4 ms	2 ms
Network Parameters	Values	
C_E —Number of recurrent excitatory connections per cell	1600	
C_I —Number of recurrent inhibitory connections per cell	400	
C_{ext} —Number of external connections per cell	3200	
v_{ext} —Spike rate from external neurons	5.00 Hz	
Synaptic Parameters	Values	
$J_{ext}^{(E)}$ —Synaptic efficacy $ext \rightarrow E$	0.070 mV	
$J_{ext}^{(I)}$ —Synaptic efficacy $ext \rightarrow I$	0.115 mV	
J_{IE} —Synaptic efficacy $E \rightarrow I$	0.080 mV	
J_{EI} —Synaptic efficacy $I \rightarrow E$	0.275 mV	
J_{II} —Synaptic efficacy $I \rightarrow I$	0.178 mV	
J_d —Depressed efficacy of plastic EE synapses	0.030 mV	
J_p —Potentiated efficacy of plastic EE synapses	gJ_d	
γ_0 —Fraction of potentiated synapses before learning	0.05	
Variable Parameters	Values	
g —Ratio between potentiated/depressed efficacies ($J_p = gJ_d$)	1–10	
ρ —Ratio between LTD/LTP probabilities ($q_- = f\rho q_+$)	0–10	
f —Fraction of E cells responding to a stimulus	0.005–0.2	
p —Number of stored memories	1–80	
Spiking Network Parameters (SIMULATION)	Values	
N_E —Number of excitatory cells	8000	
N_I —Number of inhibitory cells	2000	
c —Probability of synaptic contact	0.2	
δ —Synaptic delay	1–10 ms	
T_{stim} —Duration of visual presentation	500 ms	
T_{delay} —Interval between two successive presentations	1000 ms	
G_{stim} —External rate increase during presentation ($v_{ext} \rightarrow G_{stim}v_{ext}$)	1.5	

Notes: The first four sections are common to both. The bottom one are parameters specific to the simulation.

3.2.2 Initial Conditions. To find the solution corresponding to spontaneous activity (SA), the initial conditions are chosen to be

$$v_\alpha^s(t=0) \sim v_\alpha^n(t=0) \sim v_I(t=0) \sim v_{ext}, \quad (3.5)$$

with v_{ext} the rate of the afferent external noise (see section 2.2). For the retrieval states (delay activity, WM), if they exist, we start with

$$v_{\alpha}^s(t=0) \sim 10 \cdot v_{ext} \quad v_{\alpha}^n(t=0) \sim v_I(t=0) \sim v_{ext}, \quad (3.6)$$

which mimics the presentation of a stimulus. The behavior of the system is rather insensitive to the precise values of the initial conditions, except near critical points.

We consider three scenarios, which depend on the various network parameters:

- No selective delay activity—ergodic dynamics. The stationary rates in populations of the same multiplicity are equal, regardless of whether they are selective and independent of the initial conditions. The resulting rate distributions are denoted as $v_{\beta}(SA)$.
- Coexistence of single-item WM and spontaneous activity. The stationary solutions arrived at from initial condition 3.5 and 3.6 are different. For condition 3.5, $v_{\beta}^s(SA) = v_{\beta}^n(SA)$ for $\beta = 1, \dots, p-1$. The solution corresponding to the WM initial conditions, 3.6, has $v_{\beta}^s(WM) > v_{\beta}^n(WM)$ for $\beta = 1, \dots, p-1$. Ergodicity is broken—the final state depends on the initial condition. There will be one single-item, WM solution for each selected stimulus.⁵
- Disappearance of spontaneous activity. Upon integration with initial conditions 3.5 the system does not end up in a symmetric state as in the above two cases. Instead, it is always attracted to a WM state. Which of the p patterns is actually in the active state is determined by a fluctuation in the initial conditions or in the dynamics. Upon presentation of a stimulus, initial condition 3.6, the system ends up in a WM state corresponding to the stimulus presented.

3.2.3 Observables in MF. To obtain a compact description of the state of activity of the excitatory subnetwork, we use the rate averaged over multiplicities in the selective populations, \tilde{v}_s , and in the nonselective populations \tilde{v}_n , given by

$$\tilde{v}_s = \frac{\sum_{\beta} v_{\beta}^s \pi_s(\beta)}{\sum_{\beta} \pi_s(\beta)}, \quad \tilde{v}_n = \frac{\sum_{\beta} v_{\beta}^n \pi_n(\beta)}{\sum_{\beta} \pi_n(\beta)}. \quad (3.7)$$

We are interested primarily in determining the region in the space of the parameters in which the network is able to exhibit both the SA and the WM

⁵ There may be also multi-item solutions—states in which several populations sustain high delay activity simultaneously, as with nonoverlapping stimuli (e.g., Amit, Bernacchia, Yakovlev, & Orlov, 2003). Those could be studied by the present approach, but it goes beyond the scope of this work.

states of activity. In particular, we study the space of states of the network as we vary the ratio $g(\equiv J_p/J_d)$, between the potentiated and the depressed synaptic efficacy, varying actually J_p , at fixed J_d ; the number p of stored patterns; ρ – the ratio between the potentiation and depression synaptic transition probabilities, equation 2.1, and the coding level f , varying one parameter at a time.

3.2.4 Reduced Population Number. To reduce the number of dynamical equations in equation 2.15, we proceeded as follows. The number of relevant rates was determined starting from the mean multiplicity fp and including only the rates, in selective and nonselective populations, of multiplicity within $3\sigma (= 3\sqrt{pf})$ of the mean, as discussed in section 2.5.1.⁶ In some instances, this number of populations is cut off at the lower end, e.g., if it reaches the lowest possible multiplicity (0 or 1). We denote the reduced set of multiplicities $\{n_r\}$, where n_r is the number of subpopulations considered in the reduced treatment.

The number of equations in the dynamical system (see equation 3.4) reduces correspondingly to n_r equations, like equation 3.4, with n_r variables. Then n_r is increased to n'_r , adding one population on each side of the previously retained set of populations (where possible) and comparing the solution with the one of $\{n_r\}$. If

$$\max_{\alpha} \left\{ \frac{|v_{\alpha}^x(\{n_r\}) - v_{\alpha}^x(\{n'_r\})|}{v_{\alpha}^x(\{n_r\})}, \frac{|v_I(\{n_r\}) - v_I(\{n'_r\})|}{v_I(\{n_r\})} \right\} < \Delta_r = 10^{-2}, \quad (3.8)$$

where $\alpha \in \{n_r\}$ and $x = s, n$, then n_r is assumed as the number of populations to be retained. Otherwise, if the condition is not satisfied, the number of populations is increased and the condition checked again.

Finally, the neglected rates v_{α}^x 's are obtained, via the transduction function, by computing the mean and variance of the currents afferent on neurons of each neglected multiplicity, using the rates of the retained populations, that is,

$$\begin{cases} \mu_{\alpha}^x = C_E \left[\sum_{\beta \in \{n_r\}} J_{\alpha\beta}^{xs} v_{\beta}^s \pi_s(\beta) + \sum_{\beta \in \{n_r\}} J_{\alpha\beta}^{xn} v_{\beta}^n \pi_n(\beta) \right] + \mu_I + \mu_{ext}, \\ (\sigma_{\alpha}^x)^2 = C_E \left[\sum_{\beta \in \{n_r\}} \Delta J_{\alpha\beta}^{xs} v_{\beta}^s \pi_s(\beta) \sum_{\beta \in \{n_r\}} \Delta J_{\alpha\beta}^{xn} v_{\beta}^n \pi_n(\beta) \right] + \sigma_I^2 + \sigma_{ext}^2. \end{cases} \quad (3.9)$$

In some cases, we compare the solution with the reduced number of populations to the full MF solution ($2p + 1$ populations). In some sample

⁶ A limiting case of this approach, $f \rightarrow 0$, pf very large, was employed in Golomb et al. (1990) to study the MF of the Willshaw model.

situations, we also double-checked the convergence of our dynamics by considering the MF dynamical equations for the evolution of the means and variances of the currents, as in (Amit & Brunel, 1997a), rather than the simplified equations, equations 3.4, for the evolution of the rates.

3.2.5 Bifurcation Diagram: Varying g at Fixed p . As examples of the different possible stationary states of the network, we generate sample bifurcation diagrams. At fixed p , the synaptic structure is set up according to equations A.2. Then g is varied from 1 up. For each value of g , the MF equations, equations 3.4, are solved for the stationary states with both initial conditions, 3.5 and 3.6. We then plot the average rates \tilde{v}_s and \tilde{v}_n , equations 3.7, versus g . The phenomenology is the following:

- For $1 \leq g < g_c^{(1)}(p)$, there is a single solution at low rate, with $\tilde{v}_s \sim \tilde{v}_n$ – spontaneous activity.
- $g_c^{(1)}(p)$ is a bifurcation point. For $g_c^{(1)}(p) \leq g < g_c^{(2)}(p)$, a second solution appears, with $\tilde{v}_s \gg \tilde{v}_n$, that is, selective activity rates are significantly higher than nonselective rates. Both increase with increasing g .
- For $g \geq g_c^{(2)}(p)$, there is again a single solution: either the WM state, for $p \ll 1/f$, or symmetric (SA) at high rate, for $p > 1/f$ (see below).

3.2.6 Storage Capacity. For a given set of parameters, the network, if it has WM states, will have a critical capacity; there will be a highest value of p ($\equiv p_c$) for which the WM solutions still exist and for $p_c + 1$, there is only one stationary state that is spontaneous activity. For a given set of parameters and a given p , the synaptic couplings among the various neural populations are computed, according to equations A.2, and the corresponding steady-state solutions are obtained, as above. Keeping all parameters fixed and increasing p , we obtain p_c corresponding to that set of parameters. Then one parameter is varied at a time, giving p_c as a function of that parameter.

3.3 Simulations

3.3.1 The Network Architecture. The model network is composed of N_E excitatory and N_I inhibitory integrate-and-fire spiking neurons, equation 3.1. The direct afferent presynaptic cells of a given neuron are selected, independently and randomly, by a binary process with probability c , so that each neuron receives, on average, $cN_E = C_E$ excitatory and $cN_I = C_I$ inhibitory contacts. The structure of the connectivity remains fixed all along the simulation. The existing excitatory as well as inhibitory synapses onto inhibitory neurons are assigned a uniform value. The structuring of the excitatory-to-excitatory synapses (i.e., the statistics of the potentiated/depressed synapses) is generated according to the set of stimuli supposed to have been presented in training (see below).

To each recurrent synapse is associated a transmission delay δ —the time after which the emitted spikes are delivered to the postsynaptic cell. The synaptic delays are uniformly distributed within a bounded interval. C_{ext} excitatory contacts are afferent on each neuron from outside the network. Each is modeled by a random and independent Poissonian spike train of rate ν_{ext} . Hence, all neurons are receiving a nonselective external current $I_{ext} = J_{ext}\eta(t)$, where J_{ext} is the efficacy of the external synapses; $\eta(t)$ is a Poisson process with mean $C_{ext}\nu_{ext}$ per unit time. See Table 1.

3.3.2 The Simulation Process. The simulation consists of numerical integration of the discretized dynamical equations of the membrane depolarizations, equation 3.1, of all $(N_E + N_I)$ neurons. The temporal step is $\Delta t (= 0.05 \text{ ms})$, shorter than the average time between two successive afferent spikes. The initial distribution of depolarization in the network is set uniform at a subthreshold value. The actual value has little effect on the network dynamics—the network reaches its stationary state, corresponding to the SA state, within short relaxation times ($\sim 50 \text{ ms}$).

Spikes begin to be emitted due to the external currents. The depolarization of every neuron is sequentially updated. If $V_j(t + \Delta t) > \theta$, a spike is delivered to all postsynaptic neurons, and the depolarization is reset to $V_j = V_r$ and kept fixed for τ_{ap} milliseconds. The spike adds to the value of the depolarization of the postsynaptic neuron i , at time $t + \Delta t + \delta_{ij}$, the value J_{ij} of the corresponding synaptic efficacy. (For more details on the simulation process, see Amit & Brunel, 1997b.) The complete list of parameters is reported in Table 1.

3.3.3 Statistics of Stimuli and Learning. The p stimuli to be learned are set up, when the simulation is initialized, by a binary process: an excitatory neuron responds independently to each stimulus with probability f . Each stimulus corresponds (on average) to a pool of fN_E visually responsive excitatory neurons. These pools are kept fixed all along the simulation. Hence, one can associate with each neuron a response pattern $\{\xi_i^\mu\}$, $\mu = 1, \dots, p$, where $\xi_i^\mu = 1$ if neuron i responds to (i.e., is selective to) the stimulus number μ , and 0 otherwise. To repeat, the ξ s are not rates but merely a bookkeeping of the selectivity of the cells.

The asymptotic effect of learning is expressed in the following way. The (two-state) synapse between the presynaptic excitatory neuron j and the postsynaptic excitatory neuron i , if it exists, is set in the up state ($J_{ij} = J_p$) with probability

$$Pr(J_{ij} = J_p) = \begin{cases} \gamma_0 & \text{if } P_{ij} = D_{ij} = 0 \\ P_{ij}/(P_{ij} + f\rho D_{ij}) & \text{otherwise} \end{cases} \quad (3.10)$$

where

$$P_{ij} = \sum_{\mu=1}^p \xi_i^\mu \xi_j^\mu; \quad D_{ij} = \sum_{\mu=1}^p (1 - \xi_i^\mu) \xi_j^\mu, \quad (3.11)$$

where P_{ij} and D_{ij} are, respectively, the P and D introduced at the end of section 2.2, for the specific synapse connecting neuron j to i . γ_0 , the synaptic distribution prior to learning, is defined in equation 2.3. The synaptic matrix is generated for every value of p according to this recipe. This structuring on top of an unstructured synaptic background, follows the tradition of Brindley (1969).

3.3.4 Testing Protocol. To check the MF predictions, the network is subjected to a testing stage during which the entire set of stimuli is presented, to check which of the stimuli has a corresponding delay activity with the given synaptic structure at the given loading level. The presentation of a stimulus is expressed by an increase in the rates of external afferents to the selective cells (the corresponding pool) for an interval of T_{stim} . The rate of spikes arriving at these neurons is increased by a factor $G_{stim} > 1$, Table 1. External currents to other excitatory neurons, as well as to the inhibitory neurons, are unaltered. Accordingly, the neurons selective to a given stimulus emit at elevated rates, during the presentation of the stimulus. Note that no synaptic plasticity takes place during stimulus presentation.

The typical trial consists of a presentation interval of T_{stim} , followed by a delay interval of T_{delay} , during which none of the populations is stimulated. The presentation sequence of the stimuli is either kept fixed ($1 \rightarrow 2 \rightarrow \dots p \rightarrow 1$) or generated by choosing each stimulus to be presented independently and randomly, with probability $1/p$, until each stimulus has been presented at least once.

3.3.5 Recordings and Observables. In order to compare MF predictions with the behavior of the simulated spiking network, the average emission rates within selective and nonselective populations are estimated by equation 3.7, within each trial period, for the entire set of stimuli. The mean emission rate of a population in an interval T is estimated as the total number of spikes emitted by the neurons belonging to that population in the interval divided by T and by the total number of neurons within the population. Single-cell data are measured in a randomly selected subset of excitatory neurons (10% of the total). The subset of neurons sampled is kept fixed during the “recordings” to mimic experimental procedures. The mean emission rate of neuron i in an interval T is estimated as the number of spikes emitted by the neuron in the interval divided by T .

The mean emission rate of a neuron in the delay period is estimated starting 200 ms following the removal of the stimulus until T_{delay} after the

removal of a stimulus μ , and is denoted by v_i^μ . This is to avoid the transient following the stimulus.

From the single-cell rate estimates $\{v_i^\mu\}$, measured in the simulations, we compute the average rates in populations of cells that are selective and nonselective to stimulus μ , with a given multiplicity β , off line, as

$$V_\mu^s(\beta) = \frac{\sum_{i \in \beta} \xi_i^\mu v_i^\mu}{\sum_{i \in \beta} \xi_i^\mu}, \quad (3.12)$$

where $\sum_{i \in \beta} v_i^\mu$ is over all neurons of multiplicity β selective to stimulus μ . $V_\mu^s(\beta) \rightarrow v_\beta^s$ for each μ , as $N \rightarrow \infty$. Analogously,

$$V_\mu^n(\beta) = \frac{\sum_{i \in \beta} (1 - \xi_i^\mu) v_i^\mu}{\sum_{i \in \beta} (1 - \xi_i^\mu)}, \quad (3.13)$$

which $\rightarrow v_\beta^n$ as $N \rightarrow \infty$.

The compact average rates, that is, selective and nonselective rates averaged over all multiplicities, are obtained directly from the simulations, as

$$\begin{aligned} \langle V_\mu^s \rangle &= \frac{\sum_i \xi_i^\mu v_i^\mu}{\sum_i \xi_i^\mu} \rightarrow \frac{\sum_\beta \pi_s(\beta) v_\beta^s}{\sum_\beta \pi_s(\beta)} = \tilde{v}_s \\ \langle V_\mu^n \rangle &= \frac{\sum_i (1 - \xi_i^\mu) v_i^\mu}{\sum_i (1 - \xi_i^\mu)} \rightarrow \frac{\sum_\beta \pi_n(\beta) v_\beta^n}{\sum_\beta \pi_n(\beta)} = \tilde{v}_n \end{aligned}$$

and could also be obtained from single-cell recordings.

Note that $\langle V_\mu^s \rangle, \langle V_\mu^n \rangle$ are the analogs of the overlaps in the Hopfield model (Amit, Gutfreund, & Sompolinsky, 1985). In this way, we obtain a $\langle V_\mu^s \rangle$ and $\langle V_\mu^n \rangle$, for each μ . To compare with \tilde{v}_x of the MF analysis, equation 3.7, we compute

$$\langle \langle V^x \rangle \rangle = \frac{1}{p} \sum_\mu \langle V_\mu^x \rangle \rightarrow \tilde{v}_x. \quad (3.14)$$

The corresponding error is estimated as the standard deviation of the (p -component) vector of the $\langle V_\mu^s \rangle$'s from its mean. In some cases, when we studied only compact average rates, we presented only half of the stimulus set, to reduce simulation time.

4 Results

4.1 Bifurcation Diagrams in MF and Simulations. The equations 2.15 for the stationary states of the network, in MF, with the set of parameters

given in Table 1 and the synaptic matrix set-up as described in section 3, are solved with $2p+1$ populations for $p = 40$ and 60 . Figures 2A and 2C present the population rates, averaged over all multiplicities, in three populations: (1) the selective, active population (\tilde{v}_s); (2) the remaining nonselective neurons, including those responsive to no stimulus (\tilde{v}_n); and (3) the inhibitory neurons (v_I).

The rates are plotted versus $g \equiv J_p/J_d \geq 1$ (J_d fixed). For low values of this parameter, there is a single low-rate solution with $\tilde{v}_s \sim \tilde{v}_n$ (spontaneous activity), independent of the initial condition. Both rates, as well as the mean emission rate in the inhibitory population, increase with the potentiation level. Above a critical value $g = g_c$, which increases with p , $g_c = 7.37$ (see Figure 2A: $p = 40$), and $g_c = 8.35$ (see Figure 2C: $p = 60$), a second solution appears, in which one selective population has a persistent elevated rate ($\tilde{v}_s \gg \tilde{v}_n$), starting at 23.02 Hz in Figure 2A and 29.83 Hz in Figure 2C. Also the average, selective enhanced rate increases with increasing g .

From the microscopic simulation, we estimate (as described in section 3.3.5) the average emission rate in the selective population (i.e., neurons responsive to the stimulus, for which $\xi_i^\mu = 1$) and in the nonselective population (i.e., neurons nonresponsive to the stimulus, $\xi_i^\mu = 0$), following stimulus removal. In this way, p values for \tilde{v}_s and p values for \tilde{v}_n are obtained (see section 3). The population emission rates averaged over all p stimuli, with the corresponding error bars (standard errors over the p emission rates), are also reported in Figures 2A and 2C for five values of g —two below and two above g_c and one near g_c . The results of the numerical simulations are in good agreement with theory, except near g_c .

Figure 2B shows the distribution of the measured (simulation) selective average emission rate, during the delay period, over the $p (= 40)$ populations, for three values of g , marked (a,b,c). Far from g_c , the distribution is unimodal, either at low rates (a) or at high rates (c). By contrast, for $g \sim g_c$ (point b), the distribution is bimodal, with a peak at low rates, for populations unable to sustain WM and a peak at high rates, for those that sustain WM. The same distribution is reported in Figure 2D for $p = 60$. In this case, the distribution of the rates is bimodal at all measured points (as witnessed also by the large error bars in Figure 2C). This is due to the fact that $p = 60$ is very close to the critical capacity, $p_c(g)$, of the network and, as we show below, $p_c(g)$ does not vary much with g , in this region. At still higher values of g , there is another critical value beyond which there are two different behaviors: for low $p \ll 1/f$, the network is close to one with nonoverlapping stimuli, the SA state destabilizes, and only WM states are stable. For higher $p (> 1/f)$, the system displays only a symmetric stable state, much as the one for $g < g_c$, but at high rates. The data for these high values of g is not shown.

Figure 3 presents the detailed dependence of the rates of selective and nonselective cells, in the delay activity state (WM) versus the multiplicity β , for g above g_c , Figures 3A and 3B: $p = 40$, $g = 8$, and Figures 3C and 3D:

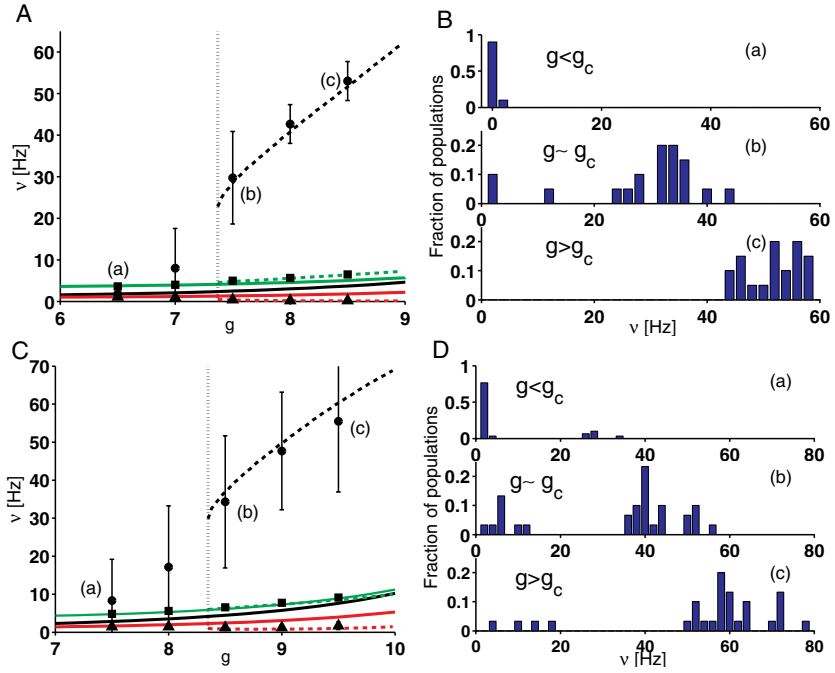


Figure 2: Bifurcation diagrams in MF and in simulation with sample (measured) rate distributions in several network states. (A, B) Networks with $p = 40$. (C, D) $p = 60$. (A, C) Average rates versus potentiation parameter g , in MF theory (curves, no fitting) and in simulation (points), in three populations: (black) selective, (red) nonselective, averaged over all multiplicities, and (green) inhibitory. Dashed curves: Retrieval (delay activity) state; continuous curves: SA state. The vertical dotted lines correspond to the bifurcation points in MF. Points in the figures on the left are average rates measured in the simulation, over an interval of 800 ms, starting 200 ms after the removal of the stimulus (see section 3). Error bars are standard errors computed over the p populations corresponding to the set of stimuli. Error bars for the inhibitory rates and the nonselective rates are too small to be noticed. (B, D) Rate histograms for selective populations, measured in the simulations, for three values of g , corresponding to the network on the left and to the point in the bifurcation diagram marked by the same letter. For $p = 40$, the rate distributions are unimodal away from the bifurcation point: $B(a)$, at low rates for $g = 6.5 < g_c$, and $B(c)$, at high rates for $g = 8.5 > g_c$. For $g = 7.5 \sim g_c$, the distribution is bimodal, due to inhomogeneities $B(b)$. For $p = 60$, all distributions are bimodal, since $60 \sim p_c$ (critical capacity) for all three sample values: $g = (7.5, 8.5, 9.5)$. See section 4.2 and Figure 6. Parameters of Table 1, with $f = 0.05$, $\rho = 1$.

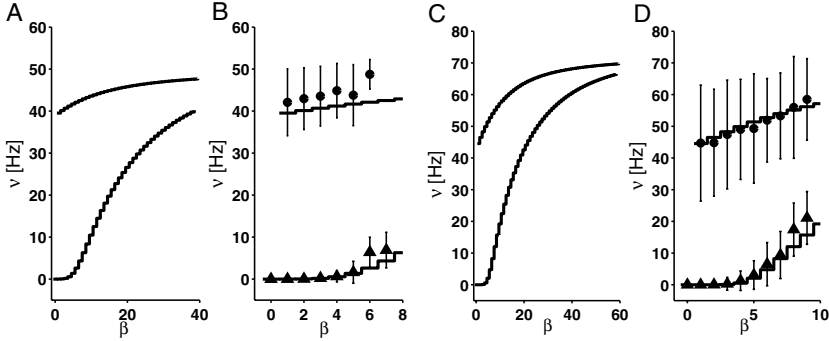


Figure 3: Average rate versus multiplicity of neural response in a delay activity state, in selective and nonselective cells, in MF and in simulations. (A, B): $p = 40$, $g = 8$; (C, D): $p = 60$, $g = 9$. (A, C): Rates for all $(2p+1)$ multiplicities (in MF); (B, D): Rates for those multiplicities on the left actually found in the simulation. $\beta \leq 7$ for $p = 40$; $\beta \leq 9$ for $p = 60$, together with the corresponding simulation results. Upper curves: selective cells; lower curves: nonselective cells. Error bars in simulation data are the standard error over the neural sample. Network parameters as in Figure 2.

$p = 60$, $g = 9$. On the left of Figures 3A and 3C are the rates in populations of all multiplicities as obtained by MF theory. On the right of Figures 3B and 3D are zooms of the part of the figures on the left for the relevant multiplicities—those actually found in the simulation ($\beta \leq 7$ for $p=40$ and $\beta \leq 9$ for $p = 60$). Shown are MF rates together with the corresponding rates measured in the simulation, each with its standard error, as found across the subset of sampled neurons (10%). Again, simulation results are in good agreement with the theory. Also, here the fluctuations for $p = 60$ are much larger (see above). The relevant rates (of the multiplicities retained in the reduction) vary relatively slowly with the multiplicity.

The large standard errors near g_c are due to inhomogeneities. These have several sources. There is structural inhomogeneity due to the random selection of the number of presynaptic afferent cells (we fix only the average number C); another source of inhomogeneity is due to the fluctuations in the coding level (around the mean fN) (see sections 3.3.1 and 3.3.3). The random connectivity produces different afferent currents to different, equivalent neurons (see Amit & Brunel, 1997b). Similarly, the randomness in coding level leads to different numbers of neurons in different (equivalent) selective populations. These fluctuations are quenched (i.e., fixed in a simulation, once the network and the stimuli have been determined). Their main effect consists in allowing, for the same value of g , some populations to be able to sustain enhanced delay activity and others not. Consequently, the critical value of g varies from population to population (see Brunel,

2000). If one were to define a critical g in the simulation as the lowest value for which all populations have persistent delay activity, it would be higher than the value obtained from MF theory, as is to be expected and as is confirmed by Figures 2A and 2C, where it is seen that for Figure 2A, it would be higher than 7.5 (compared to theoretical, MF, 7.37) and for Figure 2C higher than 9.5 (compared to theoretical 8.35). Yet, this empirical g_c may vary from simulation to simulation of the same network.

To exhibit these effects we report in Table 2 the results of simulations, with one or both of these parameters—connectivity and coding level—uniform, to compare the fluctuations with the case when they are both free (distributed as described in section 3). We do this for $p = 40$, at several values of g . Uniform connectivity implies that all neurons receive exactly the same number of afferent connections, cN_E excitatory and cN_I inhibitory; uniform coding level implies that all selective populations have the same number of neurons fN_E . As can be read from the standard errors, the inhomogeneity that more strongly affects the dynamics of the network around g_c is the variability in the coding level. When the number of neurons is set equal (at fN_E) for all populations, the standard errors are small even very near g_c , despite the variability in connectivity. They are essentially the same, as if both parameters were kept uniform. In the opposite case, uniform connectivity and random coding level, the standard errors are as large as if both variables were free. For instance, at $g = 7.5$, the standard error at uniform f and random C is 1.90 (column 3 in Table 2), while it grows to 12.28 for random coding level and uniform connectivity (column 4). Far from g_c , the various inhomogeneities only mildly affect the mean emission rate (averaged also over the stimuli) predicted by MF (last row in Table 2).

For the network tested here, the residual inhomogeneities, such as in the synaptic structuring, in the number of neurons with a given multiplicity in a given selective population, or the finite number of neurons (finite-size effects) have a rather mild effect on the average rates.

4.1.1 Effectiveness of Multiplicity Reduction. Figure 4 is an example of the effectiveness of the multiplicity reduction approach. It shows the relative errors, defined as $(\text{rate in the reduced solution} - \text{rate in full solution})/(\text{rate in full solution})$, for all rate branches in Figure 2, all along the potentiation process (g). The system memorized 60 stimuli with $f = 0.05$, so the full solution involves 121 populations. The reductions, performed around $\beta = pf = 3$, are done in three ways: with $n_r = 5$, and $n_r = 7$ and automatic, that is, until condition 3.8 is fulfilled (see section 3). For $n_r = 5$, in some branches, the relative error is as large as 15% to 20%; with $n_r = 7$, it is contained, along the entire g interval, below 2%. The automatic process constrains the error to below 1%, by construction. It is rather striking that in all three approximations, the critical value of g is equal to within about 2.5%.

Table 2: Effect of Inhomogeneities: Average Selective Emission Rates and Corresponding Standard Errors Measured in the Microscopic Simulation for Several Values of g Around g_c .

$g = \frac{J_p}{J_d}$	Both Uniform	Uniform Coding	Uniform Connection	Both Free	MF
7	3.32±1.95	2.35±1.17	11.04±11.32	7.97±9.59	2.08
7.37*	27.94±2.12	26.08±2.46	26.99±11.07	25.92±11.90	23.02
7.5	31.28±1.72	29.39±1.90	29.73±12.28	29.75±11.15	28.53
8	41.75±1.63	40.65±1.69	45.25±3.41	42.68±4.66	40.82

Notes: Network parameters as in Figure 2A. Col. 2—uniform connectivity and uniform coding level. Col. 3—uniform coding level and random connectivity. Col. 4—uniform connectivity and random coding level. Col. 5—random connectivity and random coding level. Col. 6—theoretical (MF) emission rates. The asterisk indicates the MF critical potentiation level, $g_c = 7.37$. For uniform coding level, regardless of the connectivity distribution, the standard errors are as small as when both variables are uniform, even at g_c (cols. 2 and 3). In particular, for uniform coding level, at the MF g_c , all populations exhibit persistent delay activity. By contrast, when the coding level is random, the standard errors are as large as if both parameters were free (cols. 4 and 5). These large standard errors express the fact that some populations are in a WM state, while others are in SA. Each entry in cols. 2–5 is obtained from a single simulation. The delay activity rate (in a time window of 800 ms, starting 200 ms following the removal of the stimulus; see section 3) is averaged over the cells belonging to each stimulus. The reported rate (in Hz) is the average over the 40 stimuli of the resulting population-averaged delay rates, given together with its corresponding standard error.

4.2 Storage Capacity in MF

4.2.1 Phenomenology of Storage Capacity. One expects that a given system (fixed constitutive parameters), memorizing random stimuli as stationary states, arrives at a critical point at which adding more memories results in overloading. This was foreseen by Hopfield (1982) and proved by Amit et al. (1987), for ± 1 neurons. The considerations were extended to 0–1 neurons and low coding by Tsodyks and Feigelman (1988) and Buhmann et al. (1989). Here we basically follow the logic of Amit et al. (1987): for a given set of parameters, we look for the value of p for which the equations 2.15 cease to have retrieval solutions, with $\tilde{v}_s > \tilde{v}_n$.

In Figure 5 we report the average emission rates, selective and nonselective, in the retrieval (WM) state, as a function of the number of stored memories, p . The set of parameters is that of Table 1 with $g = J_p/J_d = 9$ and $\rho = 5$, at coding level $f = 0.05$. The selective emission rate \tilde{v}_s smoothly decreases as the number of memories increases until $p = 40$. Between $p = 40$ and $p = 40+1$, the MF selective delay rate collapses to the nonselective level, that is, $\tilde{v}_s \sim \tilde{v}_n$. The retrieval solution disappears. $p_c = 40$ is the storage capacity of the network. Note that the disappearance of the delay activity at this loading level is tantamount to a blackout, that is, disappearance of delay activity for all stimuli. This is due to the fact that the slow repetitive training,

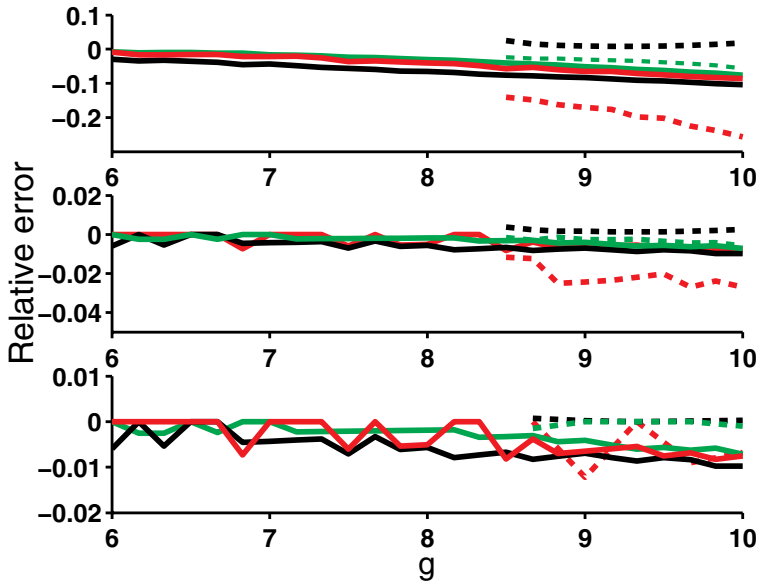


Figure 4: Convergence of MF rates for reduced population number: $p = 60$, $f = 0.05$. Relative rate differences between reduced solution and the full MF solution (121 populations) versus potentiation level g (range corresponding to the bifurcation diagram in Figure 2C). (Top) $n_r = 5$ (for nonselective (n) $\alpha = 0, 1, 2, 3, 4$, for selective (s) $\alpha = 1, 2, 3, 4$, total $9+1$ populations). (Middle) $n_r = 7$ ($n, \alpha = 0, \dots, 6$; $s, \alpha = 1, \dots, 6$, total $13+1$ populations). (Bottom) Automatic reduction, converged at $n_r = 7$ for $g < 7$; at $n_r = 8$ for $7 < g < 9$; and at $n_r = 9$ for $g > 9$ (see section 3). The relative error $< 1\%$. Color coding as in Figure 2. Full curves: spontaneous activity, dashed curves: working memory.

implied by the synaptic matrix used, renders the network fully symmetric under permutations of the different stimuli.

In Figure 5 we also present the average selective and nonselective rates in the p retrieval states, measured in the simulation of the spiking network, with the corresponding standard errors over the p rates. The results are in good agreement with theoretical predictions.

As p approaches p_c , the error bars increase. This is a signature of the bimodality of the distribution of the p selective rates, as presented, for example, in Figure 2: some populations sustain WM activity at enhanced rates, while others do not. Similar effects appear in the measured average selective rate in the spiking network, for $p > p_c$. It smoothly decreases to the spontaneous level as p increases. By contrast, in MF, the transition is abrupt, and all memories are lost together.

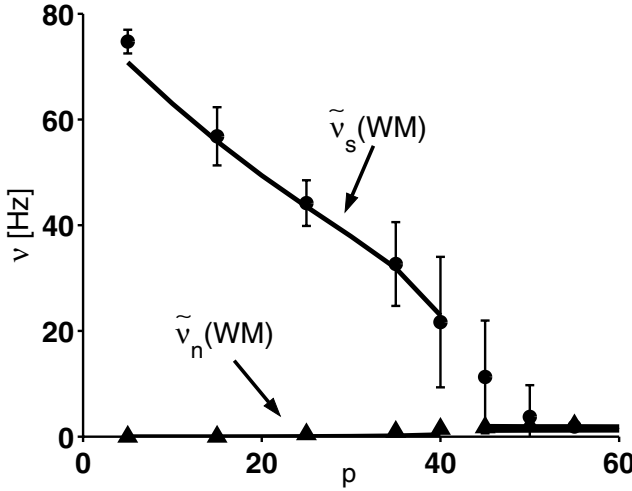


Figure 5: Selective and nonselective average rates versus number of stored memories, in MF and simulations, for $g = 9$ and $\rho = 5$, at coding level $f = 0.05$. The full curves represent average MF rates, selective (marked $\tilde{\nu}_s$) and nonselective ($\tilde{\nu}_n$), in the retrieval (WM) state. Points represent the corresponding average rates measured in the simulation. Error bars as in Figure 2. For $p > p_c (= 40)$, MF selective rate collapses to spontaneous level, $\tilde{\nu}_s \sim \tilde{\nu}_n$. The retrieval state disappears. The transition in the spiking network takes place around the value of p_c predicted by MF theory. It appears smooth because of structural fluctuations in the connectivity, synaptic structuring, coding level, and so forth (see text). For $p < p_c$, but nearby, some populations are unable to sustain WM activity. Similarly, for $p > p_c$, a subset of populations ($< p$) can still sustain elevated delay activity. See also Figure 2 and Amit (1989) and Sompolinsky (1987).

4.2.2 Memory Capacity vs. Model Parameters. We study the dependence of the storage capacity, p_c , on the ratio between the potentiated and depressed efficacies, $g = J_p/J_d$; and on the balance of potentiation to depression probabilities in the learning process $\rho \equiv q_-/(fq_+)$; on the inhibitory-to-excitatory synaptic efficacy J_{EI} , all at fixed coding level $f = 0.05$. Then we study its dependence on f , with the parameters mentioned above kept fixed.

In Figure 6 we plot p_c versus g at several values of ρ . The storage capacity p_c is obtained, at fixed g and ρ , as the largest p at which equations 2.15 still have a retrieval solution, while for $p = p_c + 1$, equations 2.15 have only the ergodic, spontaneous activity solution (see section 3). For each value of ρ , p_c rises monotonically as g increases, until it reaches a maximum at $g_{\max}(\rho)$. Near the maximum, p_c is insensitive to g and then starts to decrease. This is connected to the large fluctuations observed in the discussion of Figures 2C and 2D.

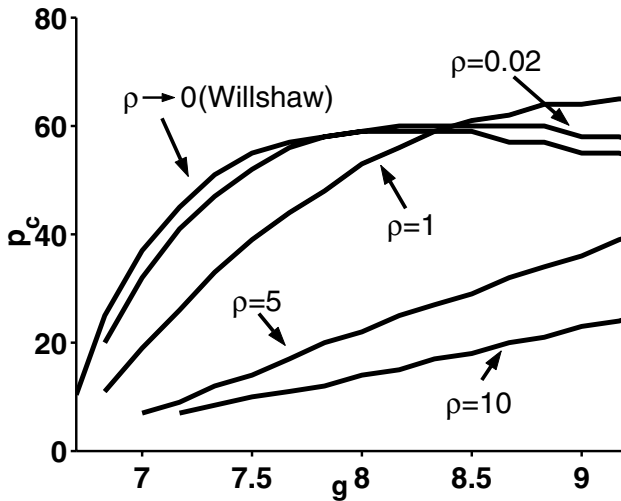


Figure 6: Storage capacity versus $g = J_p/J_d$, for several values of ρ at $f = 0.05$. p_c rises with g up to a maximum value, g_{\max} , which rises with ρ . Near g_{\max} , p_c is insensitive to the value of g . Beyond g_{\max} , the capacity begins to decrease. For g not too high, capacity increases when ρ decreases, that is, when depression is reduced relative to potentiation. The curves are not smooth due to the discrete nature of p_c .

In Figure 7 we plot p_c versus g at $\rho = 1$ for three values of the inhibitory synaptic efficacy onto excitatory neurons, J_{EI} . As can be seen, g_{\max} increases with J_{EI} , as the inhibitory currents are made stronger. As expected on the basis of the signal-to-noise analysis, the storage capacity increases as g_{\max} increases. Note that decreasing J_{EI} results in a lowering of the minimal g for which the network sustains the retrieval (WM) state. As long as the inhibitory subnetwork is able to ensure the right inhibition-excitation balance (see Amit & Brunel, 1997a), the storage capacity increases with g and decreases with increasing ρ , that is, curves with higher ρ lie lower (see Figure 6).

At fixed g , the storage capacity increases as the ratio of LTD to LTP transition probabilities decreases ($\rho \rightarrow 0$). For instance, for $g = 7.5$, the storage capacity is approximately 10 at $\rho = 10$, while it grows to about 50 when ρ decreases to 0.02 (see Figure 6). This is further elaborated in Figure 8, which shows the dependence of p_c on ρ , for $g = 8$, $g = 9$, and $g \rightarrow \infty$ (the Willshaw model, Willshaw et al., 1969). As in Figure 6, p_c is higher for higher g , and decreases with ρ for fixed g , due to excess LTD (large ρ), see e.g. (Amit & Fusi, 1992, 1994; Brunel et al., 1998). This is so because the number of depressing patterns is of order f , while the number of potentiating ones is

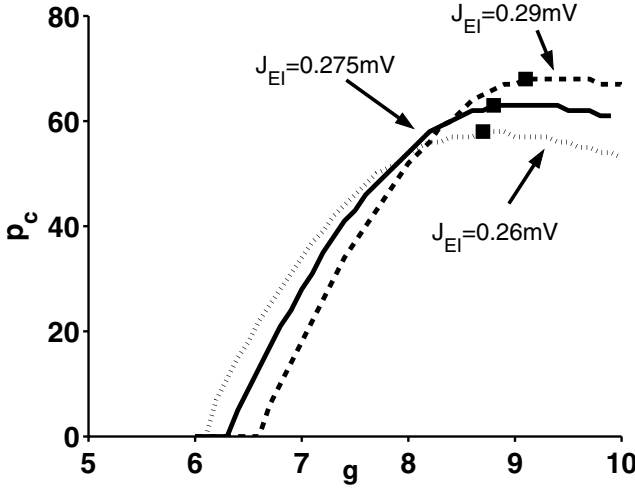


Figure 7: Storage capacity versus $g = J_p/J_d$, for several values of J_{EI} , at $\rho = 1$ and $f = 0.05$. It rises and reaches a maximum at g_{\max} and starts to decrease. As J_{EI} increases, so does g_{\max} and the capacity at g_{\max} (squares). The lower J_{EI} , the lower the bifurcation value of g , corresponding to $p_c = 1$, where WM starts.

of order f^2 , so for $f\rho \sim 1$, the resulting mean potentiation within a selective population is quite low and cannot sustain WM.

To trace the dependence of the storage capacity on the relative strength of depression, ρ , we proceed as follows: p_c was estimated using the criterion of the synaptic structuring dynamics (see Brunel et al., 1998). There the storage capacity for stationary states was estimated as the value of p at which the excess fraction of potentiated synapses within a selective population over the average potentiation level of all excitatory synapses became less than 0.5. This condition implies that p_c is the solution of the equation

$$\sum_{k=0}^p \frac{k}{k + \rho a} \frac{a^k \exp(-a)}{k} = \frac{1}{2(\rho + 1)}, \quad (4.1)$$

with $a = pf^2$. But in Brunel et al. (1998), $J_d = 0$, which in our case corresponds to $g \rightarrow \infty$. As such, it would be expected to give an overestimate of the capacity at finite g . Solving this equation at a discrete set of points $0 \leq \rho \leq 15$ gives the higher set of points in Figure 8. These points were fitted with a functional form suggested by the signal-to-noise analysis (Amit & Fusi, 1994), together with the consideration that p_c must be finite at $\rho = 0$, where the model coincides with the Willshaw model. The ansatz used was

$$p_c(\rho) = \frac{1}{1 + \rho} \left\{ A + B \cdot \ln \left(\frac{\rho^2}{1 + \rho} + C \right) \right\}. \quad (4.2)$$

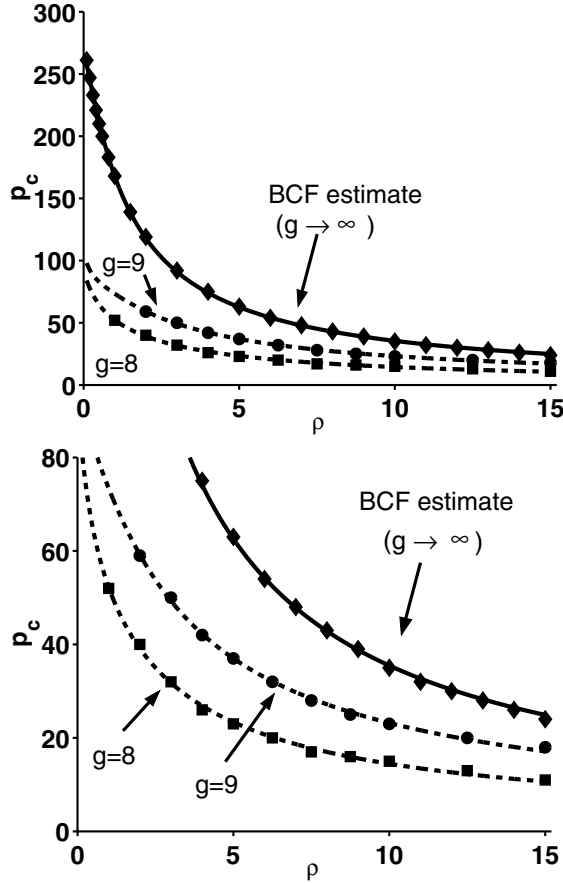


Figure 8: Storage capacity (in MF) versus ρ ($f = 0.05$). Diamonds: storage capacity of the structuring criterion, equation 4.1, (Brunel et al., 1998), at a discrete set of point $0 \leq \rho \leq 15$. Squares: MF, $g = 8$. Circles: MF, $g = 9$. Curves: Least-square fit with equation 4.2. (Top) extended range of p_c : to highlight quality of the fit for the structuring criterion, which also produces the exact value corresponding to the Willshaw model for $\rho = 0$. Coefficients: $A = 348.1$, $B = 31.76$, $C = 0.026$. (Bottom) data and fit to equation 4.2 for MF results: for $g = 8$, $A = 95.10$, $B = 27.82$, $C = 0.901$; for $g = 9$, $A = 154.4$, $B = 44.91$, $C = 0.346$.

The success of the fit (see Figure 8) led us to use the same functional form to fit the MF results. This was done for two values of g (8 and 9). The data points (MF p_c) and the fitting curves are presented in Figure 8.

Finally we study the dependence of the critical capacity on the coding level f , at fixed g for $q_- = fq_+$, that is, $\rho = 1$. If trends are well captured by

Amit and Fusi (1994), Golomb et al. (1990) and Willshaw et al. (1969), then p_c should vary as f^{-2} when f goes to zero. Figure 9 shows p_c versus f , for $g = 7$: p_c increases with decreasing f , (circles). However, when f reaches the value $f_0 (= 0.07)$, for the parameters used, the critical capacity p_c starts to fall off, as the coding level is further decreased. This is due to the fact that the selective signal scales as f , for small f , while nonselective currents as well as inhibition remain at $O(1)$. (See below and section 5.) The rising part of $p_c(f)$ is fit with the function $p_c(f) = a/f + b$ (see Figure 9, dotted line). The trend is well captured by the fit, but a fit by $1/f^2$ would be only marginally worse.

To compensate for the decrease of the signal with f , the efficacy of potentiated synapses and the selective contributions to the inhibitory neurons were scaled by $1/f$, so that all contributions to the signal remain $O(1)$ as $f \rightarrow 0$ (see also Golomb et al., 1990). This is obtained by multiplying g , as well as J_{IE}^s (the excitatory-to-inhibitory synapses from selective cells) by f_0/f , with $f_0 = 0.07$. The contributions to the variances of the currents scale correspondingly. In this case, the critical capacity continues to grow below $f < f_0$ (see Figure 9, squares). The dashed curve is a least-square fit to $a/f^2 + b$. In general, we observe that f is the most relevant variable for the variation of the capacity, rather than the number of cells N or the connectivity, much as in the Willshaw model (Willshaw et al., 1969; Golomb et al., 1990; see also section 5.2).

5 Discussion

5.1 Mean-Field Theory. The main achievement of this study is the development of an effective MF theory for the delay activity states of a network of spiking neurons, in a situation that is very close to realistic. It is realistic in several important aspects: the network is composed of randomly connected spiking IF neurons (the IF model used for the neurons fits well with in-vitro studies; see, e.g., Rauch, La Camera, Lüscher, Senn, & Fusi, 2003); neurons are divided into excitatory and inhibitory, and learning respects this division; no symmetry is assumed in the synaptic matrix; the network sustains spontaneous as well as selective activity; and it is the intensity of training that determines whether only the first or both are present (see Erickson & Desimone, 1999); the stimuli learned excite random (nonexclusive) subsets of cells in the network and the synaptic matrix that is generated is naturally connected to one that would be generated by unsupervised Hebbian learning in a system of synapses with two discrete stable states (Brunel et al., 1998).

The existence of cells responsive to several different stimuli renders the theory more complicated than previous developments, with stimuli that elicited exclusive “visual” responses (Amit & Brunel, 1997a, 1997b).⁷ The

⁷ After the submission of the article, we became aware of the experimental study of Tamura, Kaneko, Kawasaky, & Fujita (2004), which measures the multiplicities of the cells in IT cortex during stimulus presentation (e.g., their Figure 4).

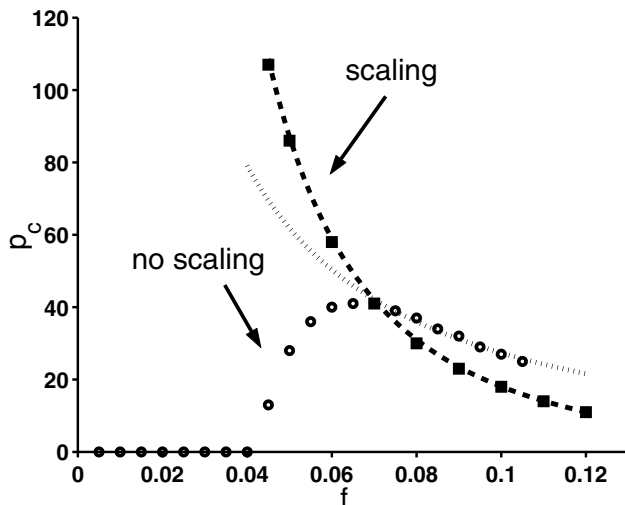


Figure 9: Storage capacity (in MF) versus coding level f . $q_- = fq_+$ ($\rho = 1$) and $g = 7$. Circles: fixed parameters (no scaling). Squares: with scaling of g and J_{IE}^s (excitatory-to-inhibitory synapses from selective populations), by f/f_0 ($f_0 = 0.07$). Dotted line: Least-square fit of the rising part of $p_c(f)$ by $a/f + b$: $a = 3.45$ and $b = -7.14$. Dashed line: Least-square fit to $a/f^2 + b$: $a = 0.23$ and $b = -4.93$.

natural populations for the study of MF theory, given overlapping stimuli, are of cells responding to a given number of stimuli. This is because the learning process envisaged respects the same population structure: it generates a synaptic structuring in which the probability of a synapse being potentiated depends only on the multiplicity of its pre- and postsynaptic neurons.

The main complication is the need to consider a coupled system of equations (for population rates) whose number grows linearly with the number of stimuli learned. However, we show that the actual number of relevant multiplicities is much smaller, due to the fact that at low coding levels, corresponding to the experimental situation, the number of neurons of multiplicity away from the mean decreases very rapidly. Hence, the number of population rates, and of the equations required, reduces sharply. The mean multiplicity is fp , and the number of required populations is of order \sqrt{fp} around the mean, where p is the number of memorized stimuli. For example, obtain precise solutions for the rates in the stationary states of the network, storing 100 memories at 5% coding level, with about 20 populations whose

coupled rates have to be solved for. The solutions are precise in the sense that they vary little when the number of populations is increased and also in their good correspondence with simulations of the underlying microscopic system of 10,000 IF spiking cells with the same synaptic matrix.

This result may open the way to a MF description of networks learning much more general sets of stimuli, not necessarily chosen at random or when the coding level of different stimuli is different. The availability of an effective MF theory is also an important tool for the exploration of the space of states of networks in experimental situations of delay response tasks of higher complexity, such as the pair-associate task (Sakai & Miyashita, 1991; Erickson & Desimone, 1999; Mongillo, Amit, & Brunel, 2003) or tasks generating context correlations (Miyashita, 1988; Amit et al., 1994). Typically, in modeling such tasks, in order to be able to explore the large parameter space, using MF theory, it was assumed that stimuli had no overlaps in the populations of neurons that coded for them. In other words, neurons had perfectly sharp tuning curves. This limitation is eliminated by our study.

Our study also opens the way for the detailed study of the learning dynamics, when synaptic plasticity is driven by spikes, modulated by the emerging synaptic structure and by unconstrained afferent stimuli. This double dynamics amplifies the number of parameters, and MF theory becomes an indispensable tool. Again, in the past, this problem was approached with nonoverlapping stimuli (see, e.g., Amit & Mongillo, 2003; Del Giudice & Mattia, 2001).

5.2 Mean Field at Vanishing ρ . It was mentioned in section 2.3 that in the limit of vanishing ρ , the synaptic structure becomes that of the Willshaw model (Willshaw et al., 1969), when $J_p = 1$, $J_d = 0$ and the initial fraction of potentiated synapses $\gamma_0 = 0$. However, Willshaw's original network was a fully synchronized system of a single-layer (feedforward) architecture. Golomb et al. (1990) developed a MF theory for a fully connected recurrent network with asynchronous Glauber dynamics and Willshaw synaptic matrix. This theory is closely related to the theory presented here, from which it can be formally obtained in the limit $\rho \rightarrow 0$. In fact, the two models share several characteristics. We defer the formal correspondences to another report.

Here we mention two of the common results. First, the dependence of the capacity on the connectivity (the number of neurons in Willshaw et al. (1969) is weak. What renders the capacity insensitive to the connectivity (N in the Willshaw model) is the fact that in both, the difference in the signals (mean current), to neurons of enhanced rate and those at low rates in a given attractor, decreases with increasing p , the number of memorized items. This is in contrast to models such as that of Amari-Hopfield (Amari, 1972; Hopfield, 1982) or Tsodyks and Feigelman (1988), in which the signal is constant and only the noise depends on p . Second, if parameters are appropriately scaled when f is varied, the storage capacity increases as

$1/f^2$ (see below and section 4). The scaling of the parameters is implicit in the capacity estimates in the Willshaw model, where the selective signal is proportional to f , and if the threshold were to remain constant as $f \rightarrow 0$, the states would have been destabilized. Hence, one could either rescale the efficacies by $1/f$, to maintain the signal constant, or scale down the threshold. This is explicitly effected in Golomb et al. (1990).

5.3 Storage Capacity, Blackout, and Palimpsest. The reliability of the MF description allows for a detailed study of the storage capacity of the network, that is, the maximal number of memories that can be stored in the synaptic couplings and retrieved by the network dynamics. The destabilization of the retrieval state depends principally on the balance between the excitatory and the inhibitory subnetworks. As the number of stored memories grows, the fraction of potentiated synapses between two selective populations, as well as within the whole excitatory subnetwork, increases. Near saturation, when a population is at elevated rates, the current afferent to the other selective populations becomes large. These, as a consequence, tend to emit at high rates, further increasing the inhibitory feedback. When the inhibitory feedback exceeds a given level, depending on the couplings within the inhibitory population and between the two subnetworks, the resulting effect is the destabilization of the retrieval state and a collapse of the network into the spontaneous activity state.

When overloading takes place, it eliminates all memories together: a blackout as in classic models (Willshaw et al., 1969; Amit et al., 1987). This, as was already mentioned, is due to the fact that the slow repeated learning renders all stimuli symmetric for the network. Yet here the situation is different, since the synaptic matrix employed derives from a realistic framework of learning (Amit & Mongillo, 2003; Fusi, 2003, for a review) and includes depression as well as potentiation. Hence, following saturation, learning of the same or a different set of stimuli can recommence and a new functioning synaptic matrix asymptotically generated. This is not part of the older paradigms of associative memory. The evolution of synaptic structuring on retraining has been studied in Brunel et al. 1998, where the speeds of learning and of forgetting were computed. Despite the fact that in that study persistent delay activity was not explicitly considered, it strongly indicates a palimpsest effect (Nadal, Toulouse, Changeux, & Dehaene, 1986); as new stimuli enter the training set, the memory of the old ones is erased to make room for the new ones. It remains to be confirmed also in the wider context of the double dynamics of neurons and synapses, where the interplay between neural activity and synaptic dynamics could generate various instabilities (see Amit & Mongillo, 2003).

Moreover, it is tempting to speculate that perhaps, given long experience, most associative networks (like those in the temporal and prefrontal lobe) work near saturation. If that were the case, one could reap yet another bonus: the emission rates of the network near saturation, for random

stimuli, become relatively low—that is, not much higher than spontaneous activity. The rates are significantly lower than those at low loading of the network (see Figure 5). This feature has been observed over a wide range of parameters for which the system was tested. The low delay rates are a feature observed in experiment and a lingering problem of neural modeling. The solutions projected for this problem are usually additional complexity in modeling, such as slow receptors and adaptive neural or synaptic elements. Here, low delay rates are a natural feature of the network with overlapping memories near saturation.

It is worth noting that the dependence of the storage capacity on network parameters like the ratio of LTD/LTP probabilities, the ratio of potentiated/depressed efficacies, and the coding level turns out to be consistent with the simple estimates of Amit and Fusi (1994) and Brunel et al. (1998), as long as the network operates in a balanced regime (excitation versus inhibition; Amit & Brunel, 1997a). For this to hold, the mean inhibitory rate must be proportional to the mean emission rate within the excitatory subnetwork. The storage capacity increases with increasing ratio of potentiated/depressed efficacies (see Figure 6) and logarithmically decreases with increasing ratio of LTD/LTP probabilities.

One also observes the increase of capacity with decreasing coding level f , foreshadowed in Willshaw et al. (1969), Tsodyks and Feigelman (1988), Buhmann et al. (1989), and Gardner (1986). On the basis of S/N considerations (Amit & Fusi, 1994), the storage capacity would increase as f^{-2} , in the limit of vanishing f and $q_- \sim fq_+$ ($\rho = 1$). The agreement of MF results with these S/N expectations is notable (see, e.g., Figure 9). Furthermore, estimating capacity by the criterion (fraction of potentiated synapses within a selective population)–(fraction of potentiated synapses within the whole excitatory subnetwork) > 0.5 , for $\rho = 1$ (Brunel et al., 1998) found $p_c \sim 0.3/f^2$, surprisingly near our $0.23/f^2$ (see Figure 9).

Our results go deeper in that they relate the potential signal separation directly to the existence of retrieval solutions of the underlying MF equations. In some sense, the signal separation, as evaluated by S/N analysis, is a necessary condition for the existence of the retrieval solution of MF equations. It may be compared to the relation between results for the Amari-Hopfield model, such as Weisbuch and Fogelman-Soulié (1985) and those of Amit et al. (1987).

Appendix: MF Populations for Selective Activity

A subpopulation of neurons in the network, corresponding to a given stimulus, may be active at selective rates, higher than the others, due to external, selective stimulation, or selective delay activity. In that case, we double the number of populations into which we divide the network. A subpopulation of neurons of a given multiplicity will be further subdivided into two (exclusive) populations—one of the neurons selective to the active stimulus

and the other for those that are not. There will be populations of multiplicity $\alpha = 1, \dots, p$, composed of neurons that are selective to the stimulus, and populations with $\alpha = 0, \dots, p - 1$ of the neurons that are not selective to the special stimulus—together, $2p$ populations of excitatory neurons. Note that the population with $\alpha = 0$ cannot be divided, because its neurons cannot be selective. Similarly, the population with $\alpha = p$ cannot, because its neurons must be selective.

These $2p$ excitatory populations are our candidates for MF homogeneous populations. We therefore assume that the rates within each of them are equal, and equal to v_β^s (for selective cells of multiplicity β) and v_β^n (for non-selective cells of the same multiplicity). The generalization of equation 2.6 is

$$\langle I_i \rangle = C_E \left[\sum_{\beta=1}^p \langle J_{ij} \rangle_\beta^s v_\beta^s \pi_s(\beta) + \sum_{\beta=0}^{p-1} \langle J_{ij} \rangle_\beta^n v_\beta^n \pi_n(\beta) \right]. \quad (\text{A.1})$$

$\pi_s(\beta)(\pi_n(\beta))$ is the probability that a selective (nonselective) neuron be of multiplicity β . $\langle J_{ij} \rangle_\beta^x$ is an average over synapses with selective ($x = s$) and nonselective ($x = n$) presynaptic neurons of multiplicity β connected to the postsynaptic neuron i .

The joint probability distributions of P potentiations and D depressions during the training with p stimuli, defined following equation 2.7, now have to be computed separately for selective and nonselective pre- and postsynaptic neurons but do not depend on the particular postsynaptic response pattern of the neuron. They depend on the multiplicity and the selectivity of the two neurons: $\psi_{\alpha\beta}^{xy}(P, D)$ where $x(y)$ is the postsynaptic(presynaptic) selectivity, while α and β are the post- and presynaptic multiplicity.

The generalization of equation 2.7 becomes,

$$J_{\alpha\beta}^{xy} = \sum_{P,D} [\gamma(P, D) J_p + (1 - \gamma(P, D)) J_d] \psi_{\alpha\beta}^{xy}(P, D), \quad (\text{A.2})$$

where xy stand for the four possibilities for having an (n,s) selectivity pair for the post- and presynaptic neurons. Following the reasoning leading to equation 2.8, one obtains, for the four possible combinations xy :

$$\psi_{\alpha\beta}^{ss}(P, D) = \frac{\binom{\alpha-1}{P-1} \binom{p-\alpha}{D}}{\binom{p-1}{\beta-1}}, P \geq 1, D = \beta - P \quad (\text{A.3})$$

$$\psi_{\alpha\beta}^{sn}(P, D) = \frac{\binom{\alpha-1}{P} \binom{p-\alpha}{D}}{\binom{p-1}{\beta}}, P \geq 0, D = \beta - P \quad (\text{A.4})$$

$$\psi_{\alpha\beta}^{ns}(P, D) = \frac{\binom{\alpha}{P} \binom{p-\alpha-1}{D-1}}{\binom{p-1}{\beta-1}}, P \geq 0, D = \beta - P \quad (\text{A.5})$$

$$\psi_{\alpha\beta}^{nm}(P, D) = \frac{\binom{\alpha}{P} \binom{p-\alpha-1}{D}}{\binom{p-1}{\beta}}, P \geq 0, D = \beta - P. \quad (\text{A.6})$$

$$\pi_s(\beta) = \binom{p-1}{\beta-1} f^\beta (1-f)^{p-\beta} \quad (\text{A.7})$$

and

$$\pi_n(\beta) = \binom{p-1}{\beta} f^\beta (1-f)^{p-\beta}. \quad (\text{A.8})$$

In the first case, the $p-1$ and $\beta-1$ are due to the fact that for the presynaptic cell, the selective bit must be on. Hence, there are $\binom{p-1}{\beta-1}$ ways of distributing the remaining $\beta-1$ 1's among the remaining $p-1$ bits. In the second case, for nonselective presynaptic neurons with multiplicity β , since the first bit must be inactive, there are $\binom{p-1}{\beta}$ ways of distributing the β 1's among the remaining $p-1$ bits.

Using equations A.3 and A.4 for selective postsynaptic neurons and equations A.5 and A.6 for nonselective ones, together with the expressions for $\pi_s(\beta)$ and $\pi_n(\beta)$ in equation A.1, one obtains for the average current afferent on selective and nonselective cells of multiplicity α , respectively:

$$\mu_\alpha^s \equiv \langle I_i \rangle = C_E \left[\sum_{\beta} J_{\alpha\beta}^{ss} v_{\beta}^s \pi_s(\beta) + \sum_{\beta} J_{\alpha\beta}^{sn} v_{\beta}^n \pi_n(\beta) \right] \quad (\text{A.9})$$

$$\mu_\alpha^n \equiv \langle I_i \rangle = C_E \left[\sum_{\beta} J_{\alpha\beta}^{ns} v_{\beta}^s \pi_s(\beta) + \sum_{\beta} J_{\alpha\beta}^{nn} v_{\beta}^n \pi_n(\beta) \right]. \quad (\text{A.10})$$

For the variances of the afferent currents, we obtain

$$(\sigma_\alpha^{xy})^2 = C_E \sum_{y=s,n} \sum_{\beta} \Delta J_{\alpha\beta}^{xy} v_{\beta}^y \pi_y(\beta), \quad (\text{A.11})$$

where

$$\Delta J_{\alpha\beta}^{xy} = \sum_{P,D} [\gamma(P, D) J_p^2 + (1 - \gamma(P, D)) J_d^2] \psi_{\alpha\beta}^{xy}(P, D). \quad (\text{A.12})$$

Finally, for completeness, we write the expressions for the mean external and inhibitory currents, μ_{ext} and μ_I :

$$\mu_{ext} = C_{ext} J_{ext} v_{ext}; \quad \mu_I = C_I J_{EI} v_I. \quad (\text{A.13})$$

The corresponding variances are given by

$$\sigma_{ext}^2 = C_{ext} J_{ext}^2 v_{ext}; \quad \sigma_I^2 = C_I J_{EI}^2 v_I. \quad (\text{A.14})$$

Acknowledgments

This study was supported by the Center of Excellence Grant “Changing Your Mind” of the Israel Science Foundation and the Center of Excellence Grant “Statistical Mechanics and Complexity” of the INFN, Roma-1. We are grateful to N. Brunel and Y. Amit for very helpful comments on the manuscript. G.L.C. thanks S. Fusi, F. Carusi, and M. Mascaró for very helpful discussions.

References

- Amari, S. I. (1972). Characteristics of random nets of analog neuron-like elements. *IEEE Trans Systems, Man and Cybernetics SMC*, 2, 643–657.
- Amit, D. (1989). *Modeling brain function*. Cambridge: Cambridge University Press.
- Amit, D. (1998). Simulation in neurobiology—theory or experiment? *TINS*, 21, 231–237.
- Amit, D., Brunel, N., & Tsodyks, M. V. (1994). Correlations of cortical Hebbian reverberations: Experiment versus theory. *Journal of Neuroscience*, 14, 6435–6445.
- Amit, D., Bernacchia, A., Yakovlev, V., & Orlov, T. (2003). Multiple-object working memory—A model for behavioral performance. *Cerebral Cortex*, 13, 435–443.
- Amit, D., & Brunel, N. (1997a). Model of global spontaneous activity and local structured (learned) delay activity during delay periods in cerebral cortex. *Cerebral Cortex*, 7, 237–252.
- Amit, D., & Brunel, N. (1997b) Dynamics of a recurrent network of spiking neurons before and following learning. *Network: Computation in Neural Systems*, 8, 373–404.
- Amit, D., Gutfreund, H., & Sompolinsky, H. (1985). Spin-glass models of neural networks. *Phys. Rev.*, A32, 1007–1018.
- Amit, D., Gutfreund, H., & Sompolinsky, H. (1987). Statistical mechanics of neural networks near saturation. *Annals of Physics*, 173, 30–67.
- Amit, D., & Fusi, S. (1992). Constraints on learning in dynamic synapses. *Network*, 3, 443–464.
- Amit, D., & Fusi, S. (1994). Learning in neural networks with material synapses. *Neural Computation*, 6, 957–982.

- Amit, D., & Mongillo, G. (2003). Spike-driven synaptic dynamics generating working memory states. *Neural Computation*, 15, 565–596.
- Amit, D., & Tsodyks, M. V. (1991). Quantitative study of attractor neural networks retrieving at low spike rates I: Substrate spikes, rates and neurons gain. *NETWORK*, 2, 259–274.
- Brindley, G. S. (1969). Nerve net models of plausible size that perform many simple learning tasks. *Proc. Roy. Soc. Lond. B*, 174, 173.
- Brunel, N. (1996). Hebbian learning of context in recurrent neural networks. *Neural Computation*, 8, 1677–1710.
- Brunel, N., & Sergi, S. (1998). Firing frequency of leaky integrate-and-fire neurons with synaptic currents dynamics. *J. Theor. Biol.*, 195, 87–95.
- Brunel, N., Carusi, F., & Fusi, S. (1998). Slow stochastic Hebbian learning of classes in recurrent neural networks. *Network: Computation in Neural Systems*, 9, 123–152.
- Brunel, N. (2000). Persistent activity and the single cell f-I curve in a cortical network model. *Network*, 11, 261–280.
- Buhmann, J., Divko, R., & Schulten, K. (1989). Associative memory with high information content. *Phys. Rev. A*, 39, 2689–2692.
- Del Giudice, P., & Mattia, M. (2001). Long- and short-term synaptic plasticity and the formation of working memory: A case study. *Neurocomputing*, 38–40, 1175–1180.
- Erickson, C. A., & Desimone, R. (1999). Responses of macaque perirhinal neurons during and after visual stimulus association learning. *J. Neuroscience*, 19, 10404–10416.
- Fulvi Mari, C. (2000). Random networks of spiking neurons: Instability in the *Xenopus* tadpole moto-neural pattern. *Physical Review Letters*, 85, 210–213.
- Fusi, S. (2003). Spike-driven synaptic plasticity for learning correlated patterns of mean firing rates. *Reviews in the Neurosciences*, 14, 73–84.
- Gardner, E. (1986). Structure of metastable states in the Hopfield model. *J. Phys. A: Math. Gen.*, 19, L1047–1052.
- Golomb, D., Rubin, N., & Sompolinsky, H. (1990). Willshaw model: Associative memory with sparse coding and low firing rates. *Phys. Rev. A*, 41, 1843–1854.
- Hopfield, J. J. (1982). Neural networks and physical systems with emergent selective computational abilities. *Proc. Natl. Acad. Sci. USA*, 79, 2554–2558.
- Hopfield, J. J. (1984). Neurons with graded response have collective computational properties like those of two-state neurons. *Proc. Natl. Acad. Sci. USA*, 81, 3088–3092.
- Kuhn, R. (1990). Statistical mechanics of networks of analogue neurons. In L. Garrido (Ed.), *Statistical mechanics of neural networks*. Berlin: Springer-Verlag.
- La Camera, G. (1999). *Apprendimento di stimoli sovrapposti in una rete di neuroni impulsanti*, Unpublished thesis, Università di Roma, La Sapienza.
- Miller, E., Erickson, C. A., & Desimone, R. (1996). Neural mechanisms of visual working memory in prefrontal cortex of the macaque. *J. Neuroscience*, 16, 5154–5167.
- Miyashita, Y. (1988). Neuronal correlate of visual associative long-term memory in the primate temporal cortex. *Nature*, 335, 817–820.

- Miyashita, Y., & Chang, H. S. (1988). Neuronal correlate of pictorial short-term memory in the primate temporal cortex. *Nature*, 331, 68–70.
- Mongillo, G., Amit, D., & Brunel, N. (2003). Retrospective and prospective persistent activity induced by Hebbian learning in a recurrent cortical network. *European Journal of Neuroscience*, 18, 2011–2024.
- Moreno, R., & Parga, N. (2004). Response of a leaky integrate-and-fire neuron to white noise input filtered by synapses with an arbitrary time constant. *Neurocomputing*, 58–60, 197–202.
- Nadal, J. P., Toulouse, G., Changeux, J. P., & Dehaene, S. (1986). Networks of formal neurons and memory palimpsests. *Europhysics Letters*, 1, 535–542.
- Rauch, A., La Camera, G., Lüscher, H. R., Senn, W., & Fusi, S. (2003). Neocortical pyramidal cells respond as integrate-and-fire neurons to in vivo-like input currents. *J. Neurophysiol.*, 90, 1598–1612.
- Ricciardi, L. (1977). *Diffusion processes and related topics in biology*. Berlin: Springer-Verlag.
- Sakai, K., & Miyashita, Y. (1991). Neural organization for the long-term memory of paired associates. *Nature*, 354, 152–155.
- Sompolinsky, H. (1987). The theory of neural networks: The Hebb rule and beyond. In L. van Hemmen & I. Morgenstern (Eds.), *Heidelberg colloquium on glassy dynamics*. Heidelberg: Springer-Verlag.
- Tamura, H., Kaneko, H., Kawasaki, K., & Fujita, I. (2004). Presumed inhibitory neurons in the macaque inferior temporal cortex: Visual response properties and functional interactions with adjacent neurons. *J. Neurophysiol.*, 91, 2782–2796.
- Tsodyks, M. V., & Feigelman, M. V. (1988). The enhanced storage capacity in neural networks with low activity level. *Europhys. Lett.*, 6, 101–105.
- Weisbuch, G., & Fogelman-Souliè, F. (1985). Scaling laws for the attractors of Hopfield networks. *J. Physique Lett.*, 46, 623–630.
- Willshaw, D., Buneman, O. P., & Longuet-Higgins, H. (1969). Nonholographic associative memory. *Nature (London)*, 222, 960–962.
- Wilson, H. R., & Cowan, J. D. (1972). Excitatory and inhibitory interactions in localized populations of model neurons. *Biophysical Journal*, 12, 1–24.

This article has been cited by:

2. Nicolas Brunel, Frédéric Lavigne. Semantic Priming in a Cortical Network Model.
Journal of Cognitive Neuroscience, ahead of print1-20. [[Abstract](#)] [[PDF](#)] [[PDF Plus](#)]